PERGAMON

International Journal of Solids and Structures 40 (2003) 6307–6333

INTERNATIONAL JOURNAL OF SOLIDS and STRUCTURES

www.elsevier.com/locate/ijsolstr

Dynamic fiber inclusions with elliptical and arbitrary cross-sections and related retarded potentials in a quasi-plane piezoelectric medium

Jizeng Wang, Thomas M. Michelitsch *, Huajian Gao

Max-Planck Institute for Metals Research, Department of Theory of Mesoscopic Phenomena, Heisenbergstrasse 3, D-70569 Stuttgart, Germany

Received 26 March 2003; received in revised form 24 June 2003

Abstract

A piezoelectric medium of transversely isotropic symmetry with continuous fiber inclusion parallel to the axis of symmetry is considered. The problem is equivalent to a two-dimensional '*quasi-plane*' piezoelectric medium containing a 2D inclusion. The inclusion is assumed to undergo a spatially uniform $\delta(t)$-type time domain transformation. The continuous fiber has elliptical, circular and arbitrary cross-sections. The solutions of the inclusion problem is expressed by scalar *potentials*. In the time domain two of these functions correspond to the *retarded potential integrals* of the inclusion. Their frequency domain representation which we shall call the '*dynamic potentials of the inclusion*' are also considered. Integral formulae are derived for continuous fiber inclusions with elliptical cross-sections. Known closed-form solutions are reproduced for circular fibers. For fibers with arbitrary cross-sections a numerical method based on Gauss quadrature is applied. High accuracy and efficiency of the numerical method is confirmed. Characteristic superposition and runtime effects for the inclusions are found.

Keywords: Dynamic inclusion problem; Retarded potential; Dynamic Green's function; Piezoelectric quasi-plane medium

1. Introduction

In smart/intelligent structures the knowledge of the dynamic characteristics of inhomogeneous materials are of high interest in supersonics, microwave technologies and in non-destructive evaluation (NDE) (e.g. Pao, 1978). Despite this high importance of the dynamical modelling there is only few work done as compared to the modelling of static mechanical properties. Talbot and Willis (1983) have analyzed the wave propagation effects caused by randomness of the microstructure. They gave estimates of dynamic material characteristics such as dispersion and attenuation.

* Corresponding author. Tel.: +49-711-689-3514; fax: +49-711-689-3512.
E-mail addresses: jz.wang@mf.mpg.de (J. Wang), michel@mf.mpg.de (T.M. Michelitsch), hjgao@mf.mpg.de (H. Gao).

0020-7683/$ - see front matter © 2003 Elsevier Ltd. All rights reserved.
doi:10.1016/S0020-7683(03)00419-0

Of special importance in the mechanics of materials is the solution of inclusion problems for inclusion geometries of interest. In statics Eshelby determined in his classical 1957 paper the strain *inside* an *elliptical inclusion* which undergoes *uniform* eigenstrain for an isotropic medium. By utilizing Dyson's theorem Rahman (2002) solved the inclusion problem of an elliptical inclusion with polynomial eigenstrain in closed compact form in terms of 'potential integrals' which are related to elliptic integrals.

The dynamical fields are of interest in the frequency and time domain. In the quasi-plane transversely isotropic medium the frequency domain solutions are determined by solutions of inhomogeneous Helmholtz equations. Frequency domain solutions we shall call '*dynamic potentials*'. Their time domain representations are the *retarded potentials* being the causal solutions of the corresponding inhomogeneous wave equation (e.g. Jackson, 1999).

There are only a few cases where closed-form solutions are available in the dynamic framework, namely for spherical inclusions (Mikata and Nemat-Nasser, 1990; Michelitsch et al., 2003a; Wang et al., 2003), for circular (cylindrical) inclusions (Cheng and Batra, 1999; Michelitsch et al., 2003a) and for the quasi-plane piezoelectric medium with circular inclusion (Michelitsch et al., 2002). In the static limit of vanishing angular frequency, the dynamic potentials are transferred into the corresponding Newtonian potentials. In the case of inhomogeneous elliptical source regions it has been shown explicitly (Michelitsch et al., 2003b) that classical results of Ferrers (1877) and Dyson (1891) are reproduced.

The present study is devoted to the quasi-plane medium with inclusions being of special engineering interest. This material system is equivalent to a three-dimensional medium containing continuous fibers. The fiber cross-section represents the two-dimensional "inclusion" in the quasi-plane medium.

This paper is organized as follows: In Section 2 we give a formulation of the dynamic inclusion problem in the 2D piezoelectric quasi-plane medium. The dynamic electroelastic fields (displacements and electric potential) are determined in terms of three types of *scalar* potentials. The time domain solution is essentially determined by two types of scalar *retarded* potentials. These potentials are convolutions of retarded Green's functions which are considered briefly in Section 3. In Section 4 we derive integral formulae for the retarded potentials for 2D source regions with elliptical shapes (corresponding to fiber inclusions with elliptical cross-sections) and of 2D elliptical rings (elliptical fiber tubes). Both the time domain and the frequency domain are considered. For circular source regions closed-form results are obtained being in agreement with those derived by Michelitsch et al. (2002, 2003a). Section 5 is devoted to the numerical evaluation based on Gauss quadrature [1] of the retarded and dynamic potentials of source regions with *arbitrary* shapes and the electroelastic dynamic fields are given in Section 6. The efficiency of the numerical method is demonstrated in Section 7 where the retarded potentials of a circular inclusion are shown to coincide with high accuracy by using both the pure numerical method and the closed-form results.

2. Dynamic inclusion problem

We consider an infinite two-dimensional '*quasi-plane*' piezoelectric medium with transversely isotropic symmetry. All field quantities depend only on the plane space vector $\mathbf{r} = (x, y)$ in the plane of transverse isotropy. We call this medium 'quasi-plane' since the displacement $\mathbf{u}(\mathbf{r}) = (u_1, u_2, u_3)$ also has an anti-plane z-component as in a 3D medium with $u_i = u_i(x, y)$ and $\frac{\partial}{\partial z}(\cdot) = 0$. It is convenient to introduce a generalized displacement field $\mathscr{U} = (u_1, u_2, u_3, u_4)$ where $u_4 = \Phi$ indicates the electric potential.

The moduli of this medium include the elastic constants $\boldsymbol{C} = \{C_{11}, C_{66}, C_{44}, C_{13}\}$, the piezoelectric constants $\boldsymbol{e} = \{e_{15}, e_{31}\}$, and the dielectric constant $\boldsymbol{\eta} = \{\eta_{11}\}$. The remaining moduli C_{33}, e_{33}, η_{33} of the 3D transversely isotropic medium are absent due to $\frac{\partial}{\partial z}(\cdot) = 0$. The linear constitutive relations are given by

[1] For a detailed discussion we refer to our recent paper, Wang et al. (2003).

$$
\begin{aligned}
&\sigma_{11} = C_{11}\frac{\partial u_1}{\partial x} + (C_{11} - 2C_{66})\frac{\partial u_2}{\partial y}; \quad \sigma_{13} = C_{44}\frac{\partial u_3}{\partial x} + e_{15}\frac{\partial u_4}{\partial x} \\
&\sigma_{12} = C_{66}\left(\frac{\partial u_1}{\partial y} + \frac{\partial u_2}{\partial x}\right); \quad \sigma_{23} = C_{44}\frac{\partial u_3}{\partial y} + e_{15}\frac{\partial u_4}{\partial y} \\
&\sigma_{22} = C_{11}\frac{\partial u_2}{\partial y} + (C_{11} - 2C_{66})\frac{\partial u_1}{\partial x}; \quad \sigma_{33} = C_{13}\left(\frac{\partial u_1}{\partial x} + \frac{\partial u_2}{\partial y}\right) \\
&D_1 = e_{15}\frac{\partial u_3}{\partial x} - \eta_{11}\frac{\partial u_4}{\partial x}; \quad D_3 = e_{31}\left(\frac{\partial u_1}{\partial x} + \frac{\partial u_2}{\partial y}\right) \\
&D_2 = e_{15}\frac{\partial u_3}{\partial y} - \eta_{11}\frac{\partial u_4}{\partial y}
\end{aligned}
\tag{1}
$$

where $\boldsymbol{\sigma}$ denotes the stress tensor and $\mathbf{D}$ the electric displacement field. The equations of motion and the charge conservation law can be compactly written as (Michelitsch et al., 2002)

$$
\left(\mathscr{T}(\nabla) - \rho\frac{\partial^2}{\partial t^2}\boldsymbol{J}\right)\mathscr{U} + \mathscr{F} = 0 \tag{2}
$$

where $\nabla = \mathbf{e}_1\frac{\partial}{\partial x} + \mathbf{e}_2\frac{\partial}{\partial y}$ denotes the plane gradient operator and $\boldsymbol{J} = \mathbf{e}_1 \otimes \mathbf{e}_1 + \mathbf{e}_2 \otimes \mathbf{e}_2 + \mathbf{e}_3 \otimes \mathbf{e}_3$ is the three-dimensional unity tensor. $\mathscr{F} = (f_1, f_2, f_3, f_4)$ denotes the generalized force density with the density of body forces f_i $(i = 1, 2, 3)$, the density of free electric charges $f_4 = -\rho_e$ and the mass density ρ. The time coordinate is denoted by t. $\mathscr{T}(\nabla)$ is a 4×4 matrix second order differential operator and has the form

$$
\mathscr{T}(\nabla) = \mathscr{T}_{\mathrm{I}}(\nabla) + \mathscr{T}_{\mathrm{II}}(\nabla) \tag{3}
$$

where

$$
\begin{aligned}
&\mathscr{T}_{\mathrm{I}}(\nabla) = C_{11}\nabla \otimes \nabla + C_{66}(\boldsymbol{\theta}\Delta - \nabla \otimes \nabla) \\
&\mathscr{T}_{\mathrm{II}}(\nabla) = \{C_{44}\mathbf{e}_3 \otimes \mathbf{e}_3 + e_{15}(\mathbf{e}_3 \otimes \mathbf{e}_4 + \mathbf{e}_4 \otimes \mathbf{e}_3) - \eta_{11}\mathbf{e}_4 \otimes \mathbf{e}_4\}\Delta
\end{aligned}
\tag{4}
$$

and $\Delta = \frac{\partial^2}{\partial x^2} + \frac{\partial^2}{\partial y^2}$ is the plane Laplace operator. The $\{\mathbf{e}_i\}$ $(i = 1, 2, 3, 4)$ are a Cartesian basis consisting of four unit vectors with $\mathscr{U} = u_i\mathbf{e}_i$ and $\boldsymbol{\theta} = \mathbf{e}_1 \otimes \mathbf{e}_1 + \mathbf{e}_2 \otimes \mathbf{e}_2$ denotes the plane unity tensor. As we observe in (4), $\mathscr{T}(\nabla)$ consists of a pure elastic part $\mathscr{T}_{\mathrm{I}}$ acting on u_1 and u_2 in the isotropy plane and a second part $\mathscr{T}_{\mathrm{II}}$ which describes the piezoelectric coupling of u_3 and u_4.

Now we consider the quasi-plane medium with 2D inclusion. We assume that the inclusion undergoes eigenstrain $\boldsymbol{\epsilon}^*$ and eigenelectric field $\boldsymbol{E}^*$. The inclusion has the *same* electroelastic moduli $\boldsymbol{C}$, $\boldsymbol{e}$, $\boldsymbol{\eta}$ and mass density ρ as the piezoelectric transversely isotropic matrix material. The eigenfields are

$$
\boldsymbol{\epsilon}^*(\mathbf{r}, t) = \rho_s(\mathbf{r})\delta(t)\boldsymbol{\epsilon}^0, \quad \mathbf{E}^*(\mathbf{r}, t) = \rho_s(\mathbf{r})\delta(t)\mathbf{E}^0 \tag{5}
$$

where $\boldsymbol{\epsilon}^0$ and $\mathbf{E}^0$ are constant. $\delta(t)$ denotes Dirac's delta function and $\delta(t)\rho_s(\mathbf{r}) = \delta(t)f(\mathbf{r})\Theta_s(\mathbf{r})$ the source density distribution [2] where $\Theta_s(\mathbf{r})$ is the characteristic function of the inclusion S. [3] Assuming the absence of external body forces, the field equations for the general displacement field $\mathscr{U}$ in the medium with inclusion then take the form of (2)

$$
\left(\mathscr{T}(\nabla) - \rho\frac{\partial^2}{\partial t^2}\boldsymbol{J}\right)\mathscr{U} + \mathscr{F}^* = 0 \tag{6}
$$

[2] The approach to be derived here allows arbitrary scalar functions ρ_s with $\int \rho_s(\mathbf{r})\mathrm{d}^2\mathbf{r} < \infty$.

[3] $\Theta_s(\mathbf{r}) = 1$, $\mathbf{r} \in S$ and $\Theta_s(\mathbf{r}) = 0$, $\mathbf{r} \notin S$.

with $\mathscr{F}^* = (f_1^*, f_2^*, f_3^*, f_4^*)$ and

$$\begin{aligned} f_i^* &= -\partial_j (C_{ijrs}\epsilon_{rs}^* - e_{kij}E_k^*) \quad (i = 1,2,3) \\ f_4^* &= -\partial_j (e_{jrs}\epsilon_{rs}^* + \eta_{jk}E_k^*) \end{aligned} \tag{7}$$

where $\partial_j = \{\frac{\partial}{\partial x}, \frac{\partial}{\partial y}\}$ and

$$\begin{aligned} f_1^* &= -\left(C_{11}\frac{\partial \epsilon_{11}^*}{\partial x} + (C_{11} - 2C_{66})\frac{\partial \epsilon_{22}^*}{\partial x} + 2C_{66}\frac{\partial \epsilon_{12}^*}{\partial y} \right) \\ f_2^* &= -\left(2C_{66}\frac{\partial \epsilon_{12}^*}{\partial x} + C_{11}\frac{\partial \epsilon_{22}^*}{\partial y} + (C_{11} - 2C_{66})\frac{\partial \epsilon_{11}^*}{\partial y} \right) \\ f_3^* &= -\left(2C_{44}\left(\frac{\partial \epsilon_{13}^*}{\partial x} + \frac{\partial \epsilon_{23}^*}{\partial y} \right) - e_{15}\left(\frac{\partial E_1^*}{\partial x} + \frac{\partial E_2^*}{\partial y} \right) \right) \\ f_4^* &= -\left(2e_{15}\left(\frac{\partial \epsilon_{13}^*}{\partial x} + \frac{\partial \epsilon_{23}^*}{\partial y} \right) + \eta_{11}\left(\frac{\partial E_1^*}{\partial x} + \frac{\partial E_2^*}{\partial y} \right) \right) \end{aligned} \tag{8}$$

The field $\mathscr{U} = (u_i)$ $(i = 1,2,3,4)$ can be expressed in terms of the Green's function $\widehat{\mathscr{G}}$, namely

$$u_i(\mathbf{r}, t) = \int \widehat{\mathscr{G}}_{ij}(\mathbf{r} - \mathbf{r}', t) f_j^*(\mathbf{r}')\, \mathrm{d}^2\mathbf{r}' \tag{9}$$

It is convenient to introduce a 4×4 potential $\mathscr{G}$ according to

$$\mathscr{G}(\mathbf{r}, t) = \int \widehat{\mathscr{G}}(\mathbf{r} - \mathbf{r}', t)\rho_s(\mathbf{r})\mathrm{d}^2\mathbf{r}' \tag{10}$$

This potential $\mathscr{G}$ then obeys

$$\left(\mathscr{T}(\nabla) - \rho\frac{\partial^2}{\partial t^2}\boldsymbol{J} \right)\mathscr{G}(\mathbf{r}, t) + \mathbf{1}\rho_s(\mathbf{r})\delta(t) = 0 \tag{11}$$

Thus the generalized displacement field of Eq. (9) becomes

$$u_k(\mathbf{r}, t) = \bar{f}_i^*(\nabla)\mathscr{G}_{ki}(\mathbf{r}, t) \tag{12}$$

where $\bar{f}_i^*(\nabla)$ $(i = 1,2,3,4)$ is the first order differential operator defined by

$$\begin{aligned} \bar{f}_i^*(\nabla) &= -(C_{ijrs}\epsilon_{rs}^0 - e_{kij}E_k^0)\partial_j \quad (i = 1,2,3) \\ \bar{f}_4^*(\nabla) &= -(e_{jrs}\epsilon_{rs}^0 + \eta_{jk}E_k^0)\partial_j \end{aligned} \tag{13}$$

or

$$\begin{aligned} \bar{f}_1^*(\nabla) &= -\left(C_{11}\epsilon_{11}^0\frac{\partial}{\partial x} + (C_{11} - 2C_{66})\epsilon_{22}^0\frac{\partial}{\partial x} + 2C_{66}\epsilon_{12}^0\frac{\partial}{\partial y} \right) \\ \bar{f}_2^*(\nabla) &= -\left(2C_{66}\epsilon_{12}^0\frac{\partial}{\partial x} + C_{11}\epsilon_{22}^0\frac{\partial}{\partial y} + (C_{11} - 2C_{66})\epsilon_{11}^0\frac{\partial}{\partial y} \right) \\ \bar{f}_3^*(\nabla) &= -\left(2C_{44}\left(\epsilon_{13}^0\frac{\partial}{\partial x} + \epsilon_{23}^0\frac{\partial}{\partial y} \right) - e_{15}\left(E_1^0\frac{\partial}{\partial x} + E_2^0\frac{\partial}{\partial y} \right) \right) \\ \bar{f}_4^*(\nabla) &= -\left(2e_{15}\left(\epsilon_{13}^0\frac{\partial}{\partial x} + \epsilon_{23}^0\frac{\partial}{\partial y} \right) + \eta_{11}\left(E_1^0\frac{\partial}{\partial x} + E_2^0\frac{\partial}{\partial y} \right) \right) \end{aligned} \tag{14}$$

The components $\mathscr{G}_{mn} = \mathscr{G}_{nm}$ $(m,n = 1,2,3,4)$ of (10) have the following physical meaning:

$\mathscr{G}_{ij}(\mathbf{R},\tau)$ $(i,j = 1,2,3)$ is the elastic displacement in i-direction at spacepoint $\mathbf{R}$ and time τ caused by the force distribution $\rho_s(\mathbf{r})\delta(t)$ acting in j-direction;
$\mathscr{G}_{i4}(\mathbf{R},\tau)$ $(i = 1,2,3)$ is the elastic displacement in i-direction at spacepoint $\mathbf{R}$ and time τ caused by the electric charge distribution $\rho_s(\mathbf{r})\delta(t)$;
$\mathscr{G}_{4j}(\mathbf{R},\tau)$ $(j = 1,2,3)$ is the electric potential at spacepoint $\mathbf{R}$ and time τ caused by the force distribution $\rho_s(\mathbf{r})\delta(t)$ acting in j-direction;
$\mathscr{G}_{44}(\mathbf{R},\tau)$ is the electric potential at spacepoint $\mathbf{R}$ and time τ caused by the electric charge distribution $\rho_s(\mathbf{r})\delta(t)$.

In view of the transversely isotropic symmetry of the operator $\mathscr{T}(\nabla)$ of Eq. (4) $\mathscr{G}$ can be decomposed into

$$\mathscr{G} = \boldsymbol{G}_{\mathrm{I}} + \boldsymbol{G}_{\mathrm{II}} \tag{15}$$

where $\boldsymbol{G}_{\mathrm{I}}$ corresponds to the pure elastic part in the isotropy plane and $\boldsymbol{G}_{\mathrm{II}}$ indicates the piezoelectric part. These parts fulfill the separate equations

$$\left(\mathscr{T}_{\mathrm{I}}(\nabla) - \boldsymbol{\theta}\rho\frac{\partial^2}{\partial t^2}\right)\boldsymbol{G}_{\mathrm{I}} + \rho_s(\mathbf{r})\delta(t)\boldsymbol{\theta} = 0 \tag{16}$$

$$\left(\mathscr{T}_{\mathrm{II}}(\nabla) - \mathbf{e}_3\otimes\mathbf{e}_3\rho\frac{\partial^2}{\partial t^2}\right)\boldsymbol{G}_{\mathrm{II}} + \rho_s(\mathbf{r})\delta(t)(\mathbf{e}_3\otimes\mathbf{e}_3 + \mathbf{e}_4\otimes\mathbf{e}_4) = 0 \tag{17}$$

Eq. (16) describes the propagation of two acoustic waves in a purely elastic 2D isotropic medium. Eq. (17) describes the wave propagation of one coupled electroacoustic axial plane shear wave which is propagating in (x,y)-plane. Its polarization is in the anti-plane 3-direction, i.e. perpendicular to the plane of transverse isotropy. [4] $\boldsymbol{G}_{\mathrm{I}}$ is obtained as (Michelitsch et al., 2002)

$$\boldsymbol{G}_{\mathrm{I}}(\mathbf{r},t) = \frac{1}{C_{66}}\boldsymbol{\theta}g_2(\mathbf{r},t) + \frac{1}{\rho}\nabla\otimes\nabla\{h_1(\mathbf{r},t) - h_2(\mathbf{r},t)\} \tag{18}$$

where g_i is determined by $(c = c_i)$

$$\left(\Delta - \frac{1}{c^2}\frac{\partial^2}{\partial t^2}\right)g + \rho_s(\mathbf{r})\delta(t) = 0 \tag{19}$$

and functions h_i are defined

$$\frac{\partial^2}{\partial t^2}h_i = g_i \tag{20}$$

where

$$c_1 = \sqrt{\frac{C_{11}}{\rho}}, \quad c_2 = \sqrt{\frac{C_{66}}{\rho}} \tag{21}$$

c_1 and c_2 indicate the wave speeds of the longitudinal and transversal polarized acoustic waves, respectively both propagating in (x,y)-plane.

[4] An extensive discussion can be found in Levin et al. (2002).

$\boldsymbol{G}_{\mathrm{II}}$ can be derived in the same way and yields (Michelitsch et al., 2002)

$$\boldsymbol{G}_{\mathrm{II}}(\mathbf{r},t)=\mathbf{e}_3\otimes\mathbf{e}_3\frac{1}{\widehat{C}_{44}}g_3(\mathbf{r},t)+(\mathbf{e}_3\otimes\mathbf{e}_4+\mathbf{e}_4\otimes\mathbf{e}_3)\frac{e_{15}}{\widehat{C}_{44}\eta_{11}}g_3(\mathbf{r},t)+\mathbf{e}_4\otimes\mathbf{e}_4\left[\frac{e_{15}^2}{\widehat{C}_{44}\eta_{11}^2}g_3(\mathbf{r},t)+\frac{1}{\eta_{11}}g_4(\mathbf{r})\delta(t)\right] \tag{22}$$

g_3 and g_4 are solutions of the equations

$$\left[\Delta-\frac{1}{c_3^2}\frac{\partial^2}{\partial t^2}\right]g_3+\rho_s(\mathbf{r})\delta(t)=0 \tag{23}$$

$$c_3=\sqrt{\frac{\widehat{C}_{44}}{\rho}},\quad \widehat{C}_{44}=C_{44}+\frac{(e_{15})^2}{\eta_{11}} \tag{24}$$

g_4 is the Newtonian potential defined by the static Poisson equation

$$-\Delta g_4+\rho_s(\mathbf{r})=0 \tag{25}$$

Eq. (22) describes an electroacoustic *coupled* shear wave propagating with velocity c_3 in (x,y)-plane with anti-plane transverse polarization $\hat{\boldsymbol{u}}_3$. The electroacoustic coupling is reflected by $\hat{\boldsymbol{u}}_4=\frac{e_{15}}{\eta_{11}}\hat{\boldsymbol{u}}_3$. Eq. (22) represents the only *electroacoustic* (piezoelectric) coupled wave existing in the quasi-plane piezoelectric medium of transversely isotropic symmetry.

With Eqs. (18) and (22), the problem of solving the field equations (11) is reduced to the determination of only three types of *scalar* potential functions, namely the retarded potential function g defined by (19), related function h of (20) and the Newtonian potential defined in (25).

In the subsequent sections we derive integral formulae for g and h for *elliptical* inclusions and propose a numerical scheme useful for the evaluation for inclusions of *arbitrary* shapes.

3. Retarded Green's functions

In this section we will give a brief introduction of the related *retarded* Green's functions. Detailed derivations can be found in the papers of Levin et al. (2002) and Michelitsch et al. (2002). We mainly focus on the causal space–time representation. The defining field equation for the retarded Green's function $\widehat{\boldsymbol{\mathscr{G}}}$ is defined by (11) when we put $\rho_s(\mathbf{r})=\delta^2(\mathbf{r})$. This retarded Green's function is fully determined by the three types of scalar Green's functions, namely (Michelitsch et al., 2002)

$$\left[\Delta-\frac{1}{c^2}\left(\frac{\partial}{\partial t}+\epsilon\right)^2\right]\hat{\boldsymbol{g}}+\delta^2(\mathbf{r})\delta(t)=0 \tag{26}$$

for the functions $\hat{\boldsymbol{g}}_{1,2,3}$ and

$$\left[\Delta-\frac{1}{c^2}\left(\frac{\partial}{\partial t}+\epsilon\right)^2\right]\left[\frac{\partial}{\partial t}+\epsilon\right]^2\hat{\boldsymbol{h}}+\delta^2(\mathbf{r})\delta(t)=0 \tag{27}$$

for $\hat{\boldsymbol{h}}_{1,2}$, where $\hat{\boldsymbol{g}}=\frac{\partial^2}{\partial t^2}\hat{\boldsymbol{h}}$, and finally

$$-\Delta\hat{g}_4+\delta^2(\mathbf{r})=0 \tag{28}$$

thus

$$\hat{g}_4(r) = \frac{1}{2\pi} \ln r \tag{29}$$

where $r = \sqrt{x^2 + y^2}$.

In Eqs. (26) and (27) we introduced an infinitesimal positive damping constant $\epsilon \to 0+$ in order to get a well defined problem leading to the *retarded* Green's functions (e.g. Levin et al., 2002).

Let us note that $\hat{\boldsymbol{h}}$ can be expressed by $\hat{\boldsymbol{g}}$ by the convolution

$$\hat{\boldsymbol{h}}(r,t) = \int_{-\infty}^{\infty} \hat{\boldsymbol{g}}(r, t-\tau)\hat{f}(\tau)\,\mathrm{d}\tau \tag{30}$$

where $\hat{f}$ is the Green's function defined by

$$\left[\frac{\partial}{\partial t} + \epsilon\right]^2 \hat{f}(t) = \delta(t) \tag{31}$$

thus

$$\hat{f}(t) = t\Theta(t)\mathrm{e}^{-\epsilon t} \tag{32}$$

where $\Theta(t)$ denotes the Heaviside step function. [5] The exponential factor $\mathrm{e}^{-\epsilon t}$ can be omitted for finite t, but has to be taken into account when integrating this function to infinity.

The Green's function $\hat{g}(r,t)$ defined in Eq. (26) is given by (e.g. Levin et al., 2002)

$$\hat{g}(r,t) = \frac{1}{2\pi} \frac{\Theta\left(t - \frac{r}{c}\right)}{\sqrt{t^2 - \left(\frac{r}{c}\right)^2}} \tag{33}$$

Expression (33) describes the physical propagation of an outgoing singular circular plane wave with propagation velocity c. The Θ-function ensures runtime causality, that is, the outgoing wave should reach a circle with radius r ($r = \sqrt{x^2 + y^2}$) around the source point $r' = 0$ only when $t = r/c$. For $t < r/c$ when the circular wave has not yet reached the circle with radius r, the Green's function is vanishing.

By evaluating integral (30) we obtain for $\hat{\boldsymbol{h}}$ the expression (Levin et al., 2002)

$$\hat{\boldsymbol{h}}(r,t) = \frac{\Theta\left(t - \frac{r}{c}\right)}{2\pi} \left\{ t \ln\left(\frac{ct}{r} + \sqrt{\frac{c^2t^2}{r^2} - 1}\right) - \sqrt{t^2 - \frac{r^2}{c^2}} \right\} \tag{34}$$

With relations (33) and (34) the *causal* dynamic Green's functions corresponding to (18) and (22) are completely determined and obtained in explicit form as (Michelitsch et al., 2002)

$$\widehat{\boldsymbol{G}}_{\mathrm{I}}(\mathbf{r},t) = \frac{1}{C_{66}} \boldsymbol{\theta} \hat{g}_2(\mathbf{r},t) + \frac{1}{\rho} \nabla \otimes \nabla \{\hat{\boldsymbol{h}}_1(\mathbf{r},t) - \hat{\boldsymbol{h}}_2(\mathbf{r},t)\} \tag{35}$$

and

$$\begin{aligned} \widehat{\boldsymbol{G}}_{\mathrm{II}}(\mathbf{r},t) = {} & \mathbf{e}_3 \otimes \mathbf{e}_3 \frac{1}{\widehat{C}_{44}} \hat{g}_3(\mathbf{r},t) + (\mathbf{e}_3 \otimes \mathbf{e}_4 + \mathbf{e}_4 \otimes \mathbf{e}_3) \frac{e_{15}}{\widehat{C}_{44}\eta_{11}} \hat{g}_3(\mathbf{r},t) \\ & + \mathbf{e}_4 \otimes \mathbf{e}_4 \left[\frac{e_{15}^2}{\widehat{C}_{44}\eta_{11}^2} \hat{g}_3(\mathbf{r},t) + \frac{1}{\eta_{11}} \hat{g}_4(\mathbf{r})\delta(t) \right] \end{aligned} \tag{36}$$

[5] $\Theta(s) = 1$ if $s > 0$ and $\Theta(s) = 0$ if $s < 0$.

where

$$\begin{aligned}
\hat{g}_i(r,t) &= \frac{1}{2\pi}\frac{\Theta\left(t-\frac{r}{c_i}\right)}{\sqrt{t^2-\left(\frac{r}{c_i}\right)^2}} \quad (i=1,2,3)\\
\hat{h}_i(r,t) &= \frac{\Theta\left(t-\frac{r}{c_i}\right)}{2\pi}\left\{t\ln\left(\frac{c_i t}{r}+\sqrt{\frac{c_i^2t^2}{r^2}-1}\right)-\sqrt{t^2-\frac{r^2}{c_i^2}}\right\} \quad (i=1,2)\\
\hat{g}_4(r) &= \frac{1}{2\pi}\ln r
\end{aligned} \tag{37}$$

and the wave velocities c_i are given in (21) and (24), respectively.

4. Retarded potential integrals for fibers and fiber tubes with elliptical cross-sections

In this section our goal is to derive potential integrals g and h defined in Eq. (19)ff. for a continuous fiber and fiber tube with semi-axes a_1, a_2. The quantity

$$p^2 = \frac{x^2}{a_1^2}+\frac{y^2}{a_2^2} \tag{38}$$

characterizes the internal $p<1$ and the external space $p>1$, respectively. We consider a wave equation of the special form $(m=0,1,2,\ldots)$ [6]

$$\left[\Delta-\frac{1}{c^2}\left(\frac{\partial}{\partial t}+\gamma\right)^2\right]g_m+\Theta(1-p)p^{2m}\delta(t)=0 \tag{39}$$

Here we introduced a phenomenological damping constant $\gamma>0$ leading to causal behavior (e.g. Levin et al., 2002). g_m can be written in the form $(\mathbf{a}=(a_1,a_2))$

$$g_m(\mathbf{r},\mathbf{a},t)=\int_0^1 p'^{2m+1}\Phi(\mathbf{r},\mathbf{a},t,p')\,\mathrm{d}p' \tag{40}$$

where Φ corresponds to a 2D elliptical ring (corresponding to a 3D continuous fiber tube with elliptical cross-section) with semi-axes $p'a_i$ obeying the equation

$$\left[\Delta-\frac{1}{c^2}\left(\frac{\partial}{\partial t}+\gamma\right)^2\right]p'\Phi(\mathbf{r},\mathbf{a},t,p')+\delta(t)\delta(p-p')=0 \tag{41}$$

Applying Fourier transformation, $\Phi(\mathbf{r},\mathbf{a},t,p')$ can be written in the form

$$p'\Phi(\mathbf{r},\mathbf{a},t,p')=\frac{1}{(2\pi)^2}\int \mathrm{e}^{\mathrm{i}\mathbf{k}\cdot\mathbf{r}}\tilde{\delta}(\mathbf{k})g(k,t)\,\mathrm{d}^2\mathbf{k} \tag{42}$$

where

$$g(k,t)=c\Theta(t)\frac{\sin ckt}{k}\mathrm{e}^{-\gamma t} \tag{43}$$

[6] Obviously $g=\sum_{m=0}a_m g_m$ then corresponds to a source density $\rho_s=\Theta(1-p)f(p^2)$ with $f(p^2)=\sum_{m=0}^{\infty}a_m p^{2m}$.

indicates the Green's function of a damped harmonic oscillator [7] of eigenfrequency ck and

$$\tilde{\delta}(\mathbf{k}) = \int \mathrm{e}^{-\mathrm{i}\mathbf{k}\cdot\mathbf{r}''}\delta(p'-p'')\mathrm{d}^2\mathbf{r}'' = 2\pi a_1 a_2 p' J_0(Kp') \tag{44}$$

$J_0(\cdot)$ indicates the Bessel function of the first kind and of order zero and $K = \sqrt{(a_1k_1)^2 + (a_2k_2)^2}$. For further evaluation the following transformation is useful (Appendix A)

$$\int_{|\hat{\mathbf{k}}|=1} f(\hat{k}_i)\,\mathrm{d}\Omega(\hat{\mathbf{k}}) = \frac{1}{a_1a_2}\int_{|\widehat{\mathbf{K}}|=1} f\left(\frac{\widehat{K}_i}{a_i}s(\widehat{\mathbf{K}})\right)s^2(\widehat{\mathbf{K}})\,\mathrm{d}\Omega(\widehat{\mathbf{K}}) \tag{45}$$

where

$$\hat{k}_i = \frac{\widehat{K}_i}{a_i}s(\widehat{\mathbf{K}}), \quad s(\widehat{\mathbf{K}}) = \frac{1}{\sqrt{\frac{\widehat{K}_1^2}{a_1^2}+\frac{\widehat{K}_2^2}{a_2^2}}} = s(\hat{\mathbf{k}}) = \sqrt{a_1^2\hat{k}_1^2 + a_2^2\hat{k}_2^2} \tag{46}$$

Eq. (42) then assumes the form

$$\Phi(\mathbf{r},\mathbf{a},t,p') = \frac{c\Theta(t)\mathrm{e}^{-\gamma t}}{(2\pi)^2}\mathrm{Re}\int_{|\widehat{\mathbf{K}}|=1} s^2(\widehat{\mathbf{K}})\,\mathrm{d}\Omega(\widehat{\mathbf{K}})\int_{|\mathbf{n}'|=1}\frac{\mathrm{d}\Omega(\mathbf{n}')}{(s(\widehat{\mathbf{K}})\widehat{\mathbf{K}}\cdot(p\mathbf{n}+p'\mathbf{n}')+ct+\mathrm{i}\epsilon)} \tag{47}$$

By using (45) this equation can be written as ($\mathbf{r} = (x_i) = x_i = pa_in_i$, $\mathbf{r}' = x_i' = a_in_i'$, $p' = 1$) and taking into account the symmetry $n_i' \leftrightarrow -n_i'$

$$\Phi(\mathbf{r},\mathbf{a},t) = \frac{a_1a_2c\Theta(t)\mathrm{e}^{-\gamma t}}{(2\pi)^2}\mathrm{Re}\int_{|\hat{\mathbf{k}}|=1}\mathrm{d}\Omega(\hat{\mathbf{k}})\int_{|\mathbf{n}'|=1}\frac{\mathrm{d}\Omega(\mathbf{n}')}{(\hat{\mathbf{k}}\cdot(\mathbf{r}-\mathbf{r}')+ct+\mathrm{i}\epsilon)} \tag{48}$$

When we first evaluate the $\hat{\mathbf{k}}$-integral [8] we obtain (Levin et al., 2002, Eqs. (A.11)ff. therein)

$$I = c\int_0^{2\pi}\frac{\mathrm{d}\varphi}{(|\mathbf{r}-\mathbf{r}'|\cos\varphi+ct+\mathrm{i}\epsilon)} = 2\pi\frac{\Theta\left(t-\frac{|\mathbf{r}-\mathbf{r}'|}{c}\right)}{\sqrt{t^2-\frac{|\mathbf{r}-\mathbf{r}'|^2}{c^2}}} \tag{49}$$

Then (48) becomes

$$\Phi(\mathbf{r},\mathbf{a},t) = a_1a_2\mathrm{e}^{-\gamma t}\int_{|\mathbf{n}'|=1}\frac{\Theta\left(t-\frac{|\mathbf{r}-\mathbf{r}'|}{c}\right)}{2\pi\sqrt{t^2-\frac{|\mathbf{r}-\mathbf{r}'|^2}{c^2}}}\,\mathrm{d}\Omega(\mathbf{n}') \tag{50}$$

which is the space–time convolution of of the Green's function $\hat{g}(r,t) = \Theta(t-\frac{r}{c})\Big/\left(2\pi\sqrt{t^2-\frac{r^2}{c^2}}\right)$ of the 2D wave equation [9] with the density $\delta(1-p)\delta(t)$. On the other hand, the $\mathbf{n}'$-integral in (48) is

$$I = \mathrm{Re}\int_0^{2\pi}\frac{\mathrm{d}\varphi}{\cos\varphi+\xi+\mathrm{i}\epsilon} \tag{51}$$

when we put $\xi = \frac{\mathbf{k}\cdot\mathbf{r}+ct}{s}$ and yields

$$I = 2\pi\frac{\Theta(\xi^2-1)}{\sqrt{\xi^2-1}}(\Theta(\xi)-\Theta(-\xi)) \tag{52}$$

[7] This Green's function fulfils $(\frac{1}{c^2}(\frac{\mathrm{d}}{\mathrm{d}t}+\gamma)^2+k^2)g(k,t) = \delta(t)$.

[8] $\hat{k}_1 = \cos\varphi$, $\hat{k}_2 = \sin\varphi$, $\mathrm{d}\Omega(\hat{\mathbf{k}}) = \mathrm{d}\varphi$.

[9] $\hat{g}$ is the solution of $(\Delta - \frac{1}{c^2}\frac{\partial^2}{\partial t^2})\hat{g}(r,t) + \delta^2(\mathbf{r})\delta(t) = 0$.

and can be also rewritten as

$$I = 2\pi \int_0^\infty \mathrm{d}\phi(\delta(\cosh\phi - \xi) - \delta(\cosh\phi + \xi)) \tag{53}$$

With (52) we find for (48) the 1D-integral

$$\Phi(\mathbf{r},\mathbf{a},t) = \frac{ca_1a_2\Theta(t)\mathrm{e}^{-\gamma t}}{2\pi} \int_{|\hat{\mathbf{k}}|=1} \frac{\Theta((\mathbf{k}\cdot\mathbf{r}+ct)^2 - s^2(\hat{\mathbf{k}}))}{\sqrt{(\mathbf{k}\cdot\mathbf{r}+ct)^2 - s^2(\hat{\mathbf{k}})}} \{\Theta(\mathbf{k}\cdot\mathbf{r}+ct) - \Theta(-[\mathbf{k}\cdot\mathbf{r}+ct])\}\mathrm{d}\Omega(\hat{\mathbf{k}}) \tag{54}$$

Using (53) yields

$$\Phi(\mathbf{r},\mathbf{a},t) = \frac{a_1a_2\Theta(t)\mathrm{e}^{-\gamma t}}{2\pi} \int_{|\hat{\mathbf{k}}|=1} \mathrm{d}\Omega(\hat{\mathbf{k}}) \int_0^\infty \mathrm{d}\phi \left\{ \delta\left(t - \frac{\hat{\mathbf{k}}\cdot\mathbf{r} + s(\hat{\mathbf{k}})\cosh\phi}{c}\right) - \delta\left(t + \frac{\hat{\mathbf{k}}\cdot\mathbf{r} + s(\hat{\mathbf{k}})\cosh\phi}{c}\right)\right\} \tag{55}$$

This expression is especially useful to obtain the frequency domain representation [10] as ($\beta = \frac{\omega+\mathrm{i}\gamma}{c}$)

$$\Phi(\mathbf{r},\mathbf{a},\beta) = \frac{a_1a_2}{2\pi} \int_{|\hat{\mathbf{k}}|=1} \mathrm{d}\Omega(\hat{\mathbf{k}}) \int_0^\infty \mathrm{d}\phi \Big(\Theta[\hat{\mathbf{k}}\cdot\mathbf{r} + s(\hat{\mathbf{k}})\cosh\phi]\mathrm{e}^{\mathrm{i}\beta(\hat{\mathbf{k}}\cdot\mathbf{r}+s(\hat{\mathbf{k}})\cosh\phi)} - \Theta[-(\hat{\mathbf{k}}\cdot\mathbf{r} + s(\hat{\mathbf{k}})\cosh\phi)]\mathrm{e}^{-\mathrm{i}\beta(\hat{\mathbf{k}}\cdot\mathbf{r}+s(\hat{\mathbf{k}})\cosh\phi)}\Big) \tag{56}$$

which assumes by using (45) together with (46)

$$\Phi(x,y,a_1,a_2,\beta) = \frac{1}{2\pi} \int_{|\widehat{\mathbf{K}}|=1} \mathrm{d}\Omega(\widehat{\mathbf{K}}) s^2(\widehat{\mathbf{K}}) \int_0^\infty \mathrm{d}\phi \Big(\Theta[p\widehat{\mathbf{K}}\cdot\mathbf{n} + \cosh\phi]\mathrm{e}^{\mathrm{i}\beta s(\widehat{\mathbf{K}})(p\widehat{\mathbf{K}}\cdot\mathbf{n}+\cosh\phi)} - \Theta[-(p\widehat{\mathbf{K}}\cdot\mathbf{n} + \cosh\phi)]\mathrm{e}^{-\mathrm{i}\beta s(\widehat{\mathbf{K}})(p\widehat{\mathbf{K}}\cdot\mathbf{n}+\cosh\phi)}\Big) \tag{57}$$

where $x_i = pa_in_i$. The dynamic potential (57) is the solution of the Helmholtz equation of a homogeneous elliptical shell being the solution of

$$(\Delta + \beta^2)\Phi + \delta(1-p) = 0 \tag{58}$$

For the *internal space* ($p < 1$) is $\cosh\phi + p\widehat{\mathbf{K}}\cdot\mathbf{n} > 0$, thus the second Θ-function in (57) is vanishing. Hence (57) becomes for the *internal space*

$$\Phi^{\mathrm{in}}(\mathbf{r},\mathbf{a},\beta) = \frac{1}{2\pi} \int_{|\widehat{\mathbf{K}}|=1} \mathrm{d}\Omega(\widehat{\mathbf{K}}) s^2(\widehat{\mathbf{K}}) \int_0^\infty \mathrm{d}\phi\, \mathrm{e}^{\mathrm{i}\beta s(\widehat{\mathbf{K}})(p\widehat{\mathbf{K}}\cdot\mathbf{n}+\cosh\phi)} \tag{59}$$

Eqs. (57) and (59) is the two-dimensional analogue of the corresponding expression of an elliptical shell in the 3D space (Michelitsch et al., 2003b; Wang et al., 2003). Taking into account the definition of the Hankel function (e.g. Courant and Hilbert, 1989) ($\beta = \frac{\omega+\mathrm{i}\gamma}{c}$, $\gamma > 0$)

$$\int_0^\infty \mathrm{e}^{\mathrm{i}\beta s\cosh\phi}\,\mathrm{d}\phi = \frac{\pi\mathrm{i}}{2} H_0^{(1)}(\beta s) \tag{60}$$

and by utilizing (45), Φ^{in} of (59) becomes ($\hat{k}_i \to n'_i$ and $x'_i = a_in'_i$, $r' = \sqrt{a_1^2n_1'^2 + a_2^2n_2'^2}$ denoting a parameterization of the radius of the 2D elliptical shell)

[10] Being defined by $\int_{-\infty}^{\infty} \mathrm{e}^{\mathrm{i}\omega t}\Phi(\mathbf{r},\mathbf{a},t)\,\mathrm{d}t$.

$$\Phi^{\text{in}}(\mathbf{r},\mathbf{a},\beta)=\frac{\mathrm{i}}{4}a_1a_2\int_{|\mathbf{n}'|=1}\mathrm{e}^{\mathrm{i}\beta\mathbf{r}\cdot\mathbf{n}'}H_0^{(1)}(\beta r')\,\mathrm{d}\Omega(\mathbf{n}') \tag{61}$$

or

$$\Phi^{\text{in}}(\mathbf{r},\mathbf{a},\beta)=a_1a_2\int_{|\mathbf{n}'|=1}\mathrm{e}^{\mathrm{i}\beta\mathbf{r}\cdot\mathbf{n}'}\hat{g}(\beta r')\,\mathrm{d}\Omega(\mathbf{n}') \tag{62}$$

where $\hat{g}(\beta r')=\frac{\mathrm{i}}{4}H_0^{(1)}(\beta r')$ denotes the Green's function of the 2D Helmholtz equation being defined by

$$(\Delta+\beta^2)\hat{g}(\beta r)+\delta^2(\mathbf{r})=0 \tag{63}$$

Eq. (61) which holds for the *internal space* is equivalent to the convolution

$$\Phi(\mathbf{r},\mathbf{a},\beta)=\frac{\mathrm{i}}{4}a_1a_2\int_{|\mathbf{n}'|=1}H_0^{(1)}(\beta|\mathbf{r}-\mathbf{r}'|)\,\mathrm{d}\Omega(\mathbf{n}') \tag{64}$$

An analogue relation as (61)–(64) exist also for an 3D elliptical shell (Michelitsch et al., 2003b). In that paper the dynamic potential of an elliptical shell (semi-axes a_1, a_2, a_3) was obtained as ($\hat{\boldsymbol{\kappa}}=(\sin\varphi\sin\theta,\cos\varphi\sin\theta,\cos\theta)$ $\mathrm{d}\Omega(\hat{\boldsymbol{\kappa}})=\sin\theta\,\mathrm{d}\theta\,\mathrm{d}\varphi$)

$$\Phi_3(x,y,z,a_1,a_2,a_3,\beta)=\frac{1}{4\pi}\int_{|\hat{\boldsymbol{\kappa}}|=1}\mathrm{d}\Omega(\hat{\boldsymbol{\kappa}})s_3^2(\hat{\boldsymbol{\kappa}})(\Theta[P\boldsymbol{\kappa}\cdot\mathbf{n}+1]\mathrm{e}^{\mathrm{i}\beta s_3(\hat{\boldsymbol{\kappa}})(P\boldsymbol{\kappa}\cdot\mathbf{n}+1)}-\Theta[-(P\boldsymbol{\kappa}\cdot\mathbf{n}+1)]\mathrm{e}^{-\mathrm{i}\beta s_3(\hat{\boldsymbol{\kappa}})(P\boldsymbol{\kappa}\cdot\mathbf{n}+1)}) \tag{65}$$

where $s_3=1\Big/\sqrt{\frac{\hat{\kappa}_1^2}{a_1^2}+\frac{\hat{\kappa}_2^2}{a_2^2}+\frac{\hat{\kappa}_3^2}{a_3^2}}$, $x_i=Pa_in_i$, and $P^2=\frac{x^2}{a_1^2}+\frac{y^2}{a_2^2}+\frac{z^2}{a_3^2}$. Eq. (65) holds in the entire space. It is easily verified that expression (57) is reproduced by the limiting transition

$$\Phi(x,y,a_1,a_2,\beta)=\lim_{a_3\to\infty}\Phi_3(x,y,z,a_1,a_2,a_3,\beta) \tag{66}$$

taking into account that $\lim_{a_3\to\infty}s_3(\hat{\boldsymbol{\kappa}})=s(\widehat{\mathbf{K}})/\sin\theta$, $P\to p$ and put $\cosh\phi=\frac{1}{\sin\theta}$. Moreover we use the symmetry of the integrand of (65) with respect to $\theta=\frac{\pi}{2}$ for $a_3\to\infty$. This transition also can also be performed directly in the time domain.

In view of (57) and (59) we observe in analogy to the 3D-case that the imaginary part $\mathrm{Im}\Phi$ is given by

$$\mathrm{Im}\Phi^{\text{in}}(\mathbf{r},\mathbf{a},\beta)=\frac{1}{2\pi}\int_{|\widehat{\mathbf{K}}|=1}\mathrm{d}\Omega(\widehat{\mathbf{K}})s^2(\widehat{\mathbf{K}})\int_0^\infty\mathrm{d}\phi\,\sin[\beta s(\widehat{\mathbf{K}})(p\widehat{\mathbf{K}}\cdot\mathbf{n}+\cosh\phi)] \tag{67}$$

which holds for both, the external and the internal space. Integrating (47) in (40) yields for the retarded potential $g=g_0(m=0)$ of a homogeneous density $\rho_s=\Theta(1-p)$ the expression $\left(\mathbf{r}'=(x_i')=(a_in_i'),\ s(\hat{\mathbf{k}})=\sqrt{a_1^2\hat{k}_1^2+a_2^2\hat{k}_2^2}\right)$

$$g(\mathbf{r},\mathbf{a},t)=\frac{ca_1a_2\Theta(t)\mathrm{e}^{-\gamma t}}{(2\pi)^2}\mathrm{Re}\int_{|\hat{\mathbf{k}}|=1}\frac{\mathrm{d}\Omega(\hat{\mathbf{k}})}{s^2(\hat{\mathbf{k}})}\int_{|\mathbf{n}'|=1}(\hat{\mathbf{k}}\cdot\hat{\mathbf{r}}')\ln[\hat{\mathbf{k}}\cdot(\mathbf{r}+\mathbf{r}')+ct+\mathrm{i}\epsilon]\,\mathrm{d}\Omega(\hat{\mathbf{n}}') \tag{68}$$

Taking into account (45) this expression can also be written as

$$g(\mathbf{r},\mathbf{a},t)=\frac{c\Theta(t)\mathrm{e}^{-\gamma t}}{(2\pi)^2}\mathrm{Re}\int_{|\widehat{\mathbf{K}}|=1}\mathrm{d}\Omega(\widehat{\mathbf{K}})s(\widehat{\mathbf{K}})\int_{|\mathbf{n}'|=1}(\widehat{\mathbf{K}}\cdot\hat{\mathbf{n}}')\ln(s(\widehat{\mathbf{K}})\widehat{\mathbf{K}}\cdot[\hat{\mathbf{n}}'+p\mathbf{n}]+ct+\mathrm{i}\epsilon)\,\mathrm{d}\Omega(\hat{\mathbf{n}}') \tag{69}$$

4.1. Homogeneous circular fiber and circular fiber tube

Consider a homogeneous fiber with circular cross-section of radius $a = a_1 = a_2$ and $\rho_s(\mathbf{r}) = \Theta(a - r)$. Eq. (68) then takes the form ($\hat{\mathbf{k}} \cdot \mathbf{r} = r\cos\varphi_1, \hat{\mathbf{k}} \cdot \mathbf{r}' = a\cos\varphi_2$)

$$g(r,a,t) = \frac{ca\Theta(t)\mathrm{e}^{-\gamma t}}{(2\pi)^2}\,\mathrm{Re}\int_0^{2\pi}\mathrm{d}\varphi_1\int_0^{2\pi}\cos\varphi_2\ln[r\cos\varphi_1 + a\cos\varphi_2 + ct + \mathrm{i}\epsilon]\,\mathrm{d}\varphi_2 \tag{70}$$

coinciding with the expression obtained by Michelitsch et al. (2002) (Eq. (5.15) therein).

It is illuminating to return to (48) which becomes

$$\Phi(r,a,t) = \frac{c\Theta(t)\mathrm{e}^{-\gamma t}a^2}{(2\pi)^2}\int_0^{2\pi}\int_0^{2\pi}\frac{\mathrm{d}\varphi_1\,\mathrm{d}\varphi_2}{(r\cos\varphi_1 + a\cos\varphi_2 + ct + \mathrm{i}\epsilon)} \tag{71}$$

Except for the multiplier a^2 the variables r and a occur symmetrically in this expression. This is a consequence of Ivory's theorem. [11] That is, we only need to evaluate above expression for the internal space $r < a$ to obtain Φ also for the external space $r > a$ by exchanging r and a in the expression Φ/a^2. For $a = a_1 = a_2$, (59) becomes ($p\widehat{\mathbf{K}} \cdot \mathbf{n} + \cosh\phi > 0$)

$$\Phi^{\mathrm{in}}(r,a,\beta) = \frac{a^2}{2\pi}\int_0^{2\pi}\mathrm{e}^{\mathrm{i}\beta r\cos\varphi}\mathrm{d}\varphi\int_0^{\infty}\mathrm{e}^{\mathrm{i}\beta a\cosh\phi}\mathrm{d}\phi \tag{72}$$

or

$$\Phi^{\mathrm{in}}(r,a,\beta) = \frac{\pi\mathrm{i}a^2}{2}J_0(\beta r)H_0^{(1)}(\beta a) \tag{73}$$

where J_0 and $H_0^{(1)}$ denote the Bessel- and Hankel functions, respectively. Exchanging r and a in the expression Φ^{in}/a^2 we obtain for the *external space* the expression

$$\Phi^{\mathrm{out}}(r,a,\beta) = \frac{\pi\mathrm{i}a^2}{2}J_0(\beta a)H_0^{(1)}(\beta r) \tag{74}$$

This equation can also be written as

$$\Phi^{\mathrm{out}}(r,a,\beta) = \hat{g}(r,\beta)\tilde{\delta}(\beta,a) \tag{75}$$

where $\hat{g}(r,\beta) = \frac{\mathrm{i}}{4}H_0^{(1)}(\beta r)$ is the Green's function of the 2D Helmholtz equation and $\tilde{\delta}(\beta,a)$ is the Fourier transform of the density $\delta(1-p)$ ($p = r/a$)

$$\tilde{\delta}(\beta,a) = \int\delta(1-p)\mathrm{e}^{-\mathrm{i}\beta\hat{\mathbf{k}}\cdot\mathbf{r}}\mathrm{d}^2\mathbf{r} = 2\pi a^2 J_0(\beta a) \tag{76}$$

Corresponding relations hold in the 2D- and 3D space when the source density function has *spherical symmetry* (e.g. Michelitsch et al., 2002, Eq. (A.22); Michelitsch et al., 2003a, Eq. (4.16)). In accordance with (67) we find for both expressions the same imaginary part, namely ($\mathrm{Re}H_0^{(1)} = J_0$)

$$\mathrm{Im}\Phi(r,a,\beta) = \frac{\pi a^2}{2}J_0(\beta a)J_0(\beta r) \tag{77}$$

which is symmetric with respect to $r \leftrightarrow a$ as a consequence of Ivory's theorem. Using expression (55) the dynamic potentials of heterogeneous fiber sources of the form $\rho_s = f(p^2)\Theta(1-p)$ with elliptical cross-

[11] For a discussion of the Ivory's theorem, see e.g. Routh (1982).

sections can be generated via integral (40). For a homogeneous continuous fiber of circular cross-section ($\rho_s = \Theta(a-r)$) evaluation of (40) in the frequency domain yields for the *internal space* ($r < a$)

$$g(r,a,\beta) = g^{\text{in}}(r,a,\beta) = \frac{1}{\beta^2}\left[\frac{\mathrm{i}\pi}{2}\beta a J_0(\beta r)H_1^{(1)}(\beta a) - 1\right] \tag{78}$$

and for the *external space* ($r > a$)

$$g(r,a,\beta) = g^{\text{out}}(r,a,\beta) = \frac{\pi \mathrm{i} a}{2\beta}H_0^{(1)}(\beta r)J_1(\beta a) \tag{79}$$

where $H_n^{(1)}(s)$ denotes the Hankel- and $J_n(s)$ the Bessel functions. Taking into account (20) we have $h(r,a,\beta) = -g(r,a,\beta)/(c\beta)^2$. Expressions (78) and (79) coincide with those obtained by Michelitsch et al. (2002, 2003a). Moreover, we verify that (73), (74) and (78), (79) are related by

$$\Phi(r,a,\beta) = a\frac{\mathrm{d}}{\mathrm{d}a}g(r,a,\beta) \tag{80}$$

reflecting the fact that ($a\frac{\mathrm{d}}{\mathrm{d}a}\Theta(a-r) = \delta(1-p)$, $p = r/a$). Eqs. (78) and (79) are solutions of

$$(\Delta + \beta^2)g(r,a,\beta) + \Theta(a-r) = 0 \tag{81}$$

which is transferred by application of the operator $a\frac{\mathrm{d}}{\mathrm{d}a}$ into ($a\frac{\mathrm{d}}{\mathrm{d}a}g(r,a,\beta) = \Phi(r,a,\beta)$)

$$(\Delta + \beta^2)\Phi(r,a,\beta) + \delta(1-p) = 0 \tag{82}$$

In the following sections a numerical method based on Gauss quadrature is applied being useful for inclusions with arbitrary shapes.

5. Numerical evaluation for fiber inclusion with arbitrary cross-section

In this section we derive a convenient representation for numerical evaluations of the retarded potentials $\boldsymbol{G}_{\text{I}}$ and $\boldsymbol{G}_{\text{II}}$ defined in (18) and (22), respectively. We mainly focus on numerical evaluation of fiber inclusions with *arbitrary* cross-sections. [12] The numerical method we propose is based on Gauss quadrature and applicable in the same way for both the space–time- and the space–frequency domain. In order to study the effect of different inclusion shapes we focus on fibers with unit density $\rho_s = \Theta_s(\mathbf{r})$. The method is also useful for inhomogeneous densities $\rho_s(\mathbf{r}) = \Theta_s(\mathbf{r})f(\mathbf{r})$ in the 2D and 3D space (Wang et al., 2003). We specify the boundary of the 2D source region S as the curve in (x,y)-plane fulfilling $F(x,y) = F(\mathbf{r}) = 0$.

The solutions of Eqs. (19), (20), (23) and (25) in the space–time representation have the form

$$g_i(\mathbf{r},t) = \int_S \hat{g}_i(|\mathbf{r}-\mathbf{r}'|,t)\rho_s(\mathbf{r}')\mathrm{d}^2\mathbf{r}' \quad (i = 1,2,3) \tag{83}$$

$$h_i(\mathbf{r},t) = \int_S \hat{h}_i(|\mathbf{r}-\mathbf{r}'|,t)\rho_s(\mathbf{r}')\mathrm{d}^2\mathbf{r}' \quad (i = 1,2) \tag{84}$$

$$g_4(\mathbf{r}) = \int_S \hat{g}_4(|\mathbf{r}-\mathbf{r}'|)\rho_s(\mathbf{r}')\mathrm{d}^2\mathbf{r}' \tag{85}$$

where $\hat{g}_i$, $\hat{h}_i$, $\hat{g}_4$ can be found in (37).

[12] There will be only slight restrictions to the nature of the boundary curve (Eqs. (86) and (87)).

Let $\mathbf{s} = \mathbf{r}' - \mathbf{r}$, thus the boundary of the inclusion S in the new coordinate system is characterized by $F(\mathbf{s}+\mathbf{r}) = 0$. Let us introduce a parameterization of the boundary of the fiber S which can be written in polar coordinates

$$\mathbf{s} = r_s \hat{\mathbf{e}}_s(\theta) \tag{86}$$

with $\hat{\mathbf{e}}_s(\theta) = (\cos\theta, \sin\theta)$ and

$$r_s = P(\theta, \mathbf{r}), \quad \theta \in [\alpha(\mathbf{r}), \beta(\mathbf{r})] \tag{87}$$

We should note that we confine here on such 'regular' cases where *each* spacepoint on the boundary is characterized by a unique pair (r_s, θ), that is we assume r_s is a unique function of θ. [13]

In (87) we have to distinguish the *internal space* ($\Theta_s(\mathbf{r}) = 1$) and the *external* space ($\Theta_s(\mathbf{r}) = 0$), respectively. If spacepoint $\mathbf{r}$ is located outside of S then in general $[\alpha(\mathbf{r}), \beta(\mathbf{r})] \in [0, 2\pi]$ are functions of $\mathbf{r}$ where two branches $P_u(\theta, \mathbf{r}), P_l(\theta, \mathbf{r})$ occur in (87) parameterizing the upper and lower boundary curves of S. If the spacepoint $\mathbf{r}$ is located *inside* S only *one* branch $r_s = P_u(\theta, \mathbf{r})$ exists where $P_l(\theta, \mathbf{r}) = 0$ thus $\alpha = 0$, $\beta = 2\pi$ in (87). Evaluating integrals (83)–(85) by using (86) and (87) yields ($\gamma = 0$)

$$\begin{aligned} g_i(\mathbf{r}, t) &= \frac{c_i}{2\pi} \int_\alpha^\beta \mathrm{d}\theta \int_{P_l}^{P_u} \mathrm{d}r_s \left[\frac{r_s \Theta(c_i t - r_s)}{\sqrt{c_i^2 t^2 - r_s^2}} \right] = \frac{c_i}{2\pi} \Theta(c_i t - P) \int_\alpha^\beta \mathrm{d}\theta \int_{H_{il}}^{H_{iu}} \mathrm{d}r_s \left[\frac{r_s}{\sqrt{c_i^2 t^2 - r_s^2}} \right] \\ &= \int_\alpha^\beta \mathrm{d}\theta \Phi_i(\theta, \mathbf{r}, t) \end{aligned} \tag{88}$$

$$\begin{aligned} h_i(\mathbf{r}, t) &= \frac{1}{2\pi} \int_\alpha^\beta \mathrm{d}\theta \int_{P_l}^{P_u} \mathrm{d}r_s \left[t \ln\left(\frac{c_i t}{r_s} + \sqrt{\frac{c_i^2 t^2}{r_s^2} - 1} \right) - \sqrt{t^2 - \frac{r_s^2}{c_i^2}} \right] \Theta(c_i t - r_s) r_s \\ &= \frac{1}{2\pi} \Theta(c_i t - P) \int_\alpha^\beta \mathrm{d}\theta \int_{H_{il}}^{H_{iu}} \mathrm{d}r_s \left[t \ln\left(\frac{c_i t}{r_s} + \sqrt{\frac{c_i^2 t^2}{r_s^2} - 1} \right) - \sqrt{t^2 - \frac{r_s^2}{c_i^2}} \right] r_s = \int_\alpha^\beta \mathrm{d}\theta \Upsilon_i(\theta, \mathbf{r}, t) \end{aligned} \tag{89}$$

$$\begin{aligned} g_4(\mathbf{r}) &= \frac{1}{2\pi} \int_\alpha^\beta \mathrm{d}\theta \int_{P_l}^{P_u} \mathrm{d}r_s [r_s \ln(r_s)] = \frac{1}{2\pi} \int_\alpha^\beta \mathrm{d}\theta \left[\frac{P_l^2}{4} - \frac{P_u^2}{4} + \frac{1}{2} P_u^2 \ln(P_u) - \frac{1}{2} P_l^2 \ln(P_l) \right] \\ &= \int_\alpha^\beta \mathrm{d}\theta \Psi(\theta, \mathbf{r}, t) \end{aligned} \tag{90}$$

where

$$\begin{aligned} \Phi_i(\theta, \mathbf{r}, t) &= \frac{c_i}{2\pi} \Theta(c_i t - P) \left[\sqrt{c_i^2 t^2 - H_{il}^2} - \sqrt{c_i^2 t^2 - H_{iu}^2} \right] \\ \Upsilon_i(\theta, \mathbf{r}, t) &= \Theta(c_i t - P) \left\{ \left[-\frac{1}{12\pi c_i} (c_i^2 t^2 + 2H_{iu}^2) \sqrt{c_i^2 t^2 - H_{iu}^2} + \frac{1}{4\pi} H_{iu}^2 t \ln\left(\frac{c_i t}{H_{iu}} + \sqrt{\frac{c_i^2 t^2}{H_{iu}^2} - 1} \right) \right] \right. \\ &\quad \left. - \left[-\frac{1}{12\pi c_i} (c_i^2 t^2 + 2H_{il}^2) \sqrt{c_i^2 t^2 - H_{il}^2} + \frac{1}{4\pi} H_{il}^2 t \ln\left(\frac{c_i t}{H_{il}} + \sqrt{\frac{c_i^2 t^2}{H_{il}^2} - 1} \right) \right] \right\} \\ \Psi(\theta, \mathbf{r}) &= \frac{1}{2\pi} \left[\frac{P_l^2}{4} - \frac{P_u^2}{4} + \frac{1}{2} P_u^2 \ln(P_u) - \frac{1}{2} P_l^2 \ln(P_l) \right] \end{aligned} \tag{91}$$

[13] Cases of ambiguous r_s may occur when the boundary contains coves. Such irregular cases are not considered here.

where $P(\mathbf{r}) = \min_\theta[P_l(\theta,\mathbf{r})]$, and $H_{il}(\theta,\mathbf{r}) = \min[c_i t, P_l(\theta,\mathbf{r})]$, $H_{iu}(\theta,\mathbf{r}) = \min[c_i t, P_u(\theta,\mathbf{r})]$. If we define the region $\Omega_i = \{(r_s,\theta)|r_s \leqslant c_i t,\ \theta \in [0,2\pi]\}$, $\Xi = \Omega_i \cap S$, then H_{il} and H_{iu} are the boundary of Ξ. The boundary of a region is assumed to be continuous in the variable θ. Then H_{il}, H_{iu}, Φ_i, Υ_i, Ψ are also continuous functions of θ. In order to represent integrals (88)–(90) in series form useful for numerics, we use the Gauss–Chebyshev quadrature formula (e.g. Press et al., 1992). The abscissa and weights for domain $[\alpha,\beta]$ are

$$\begin{aligned} s_k &= \frac{\beta-\alpha}{2}\cos\left(\frac{\pi k-\pi/2}{N}\right)+\frac{\alpha+\beta}{2} \\ w_k &= \pi\frac{\beta-\alpha}{2N}\sin\left(\frac{\pi k-\pi/2}{N}\right) \quad (k=1,2,3,\ldots,N) \end{aligned} \tag{92}$$

Thus, for a function $v(\theta) \in \mathbf{C}[\alpha,\beta]$ we have

$$\int_\alpha^\beta v(\theta)\,\mathrm{d}\theta = \lim_{N\to\infty}\sum_{k=1}^{N} w_k v(s_k) \tag{93}$$

Eq. (93) can be proofed by the theorem of Davis and Rabinowitz (1984). Therefore, (88) and (90) can be replaced by

$$g_i(\mathbf{r},t) = \int_\alpha^\beta \mathrm{d}\theta\Phi_i(\theta,\mathbf{r},t) = \lim_{N\to\infty}\sum_{k=1}^{N} w_k\Phi_i(s_k,\mathbf{r},t) \tag{94}$$

$$h_i(\mathbf{r},t) = \int_\alpha^\beta \mathrm{d}\theta\Upsilon_i(\theta,\mathbf{r},t) = \lim_{N\to\infty}\sum_{k=1}^{N} w_k\Upsilon_i(s_k,\mathbf{r},t) \tag{95}$$

$$g_4(\mathbf{r}) = \int_\alpha^\beta \mathrm{d}\theta\Psi(\theta,\mathbf{r}) = \lim_{N\to\infty}\sum_{k=1}^{N} w_k\Psi(s_k,\mathbf{r}) \tag{96}$$

With results (94)–(96) we can write for the dynamic potentials $\boldsymbol{G}_{\mathrm{I}}$ and $\boldsymbol{G}_{\mathrm{II}}$ of Eqs. (18) and (22) in the space–time domain

$$\begin{aligned} \boldsymbol{G}_{\mathrm{I}}(\mathbf{r},t) &= \frac{1}{C_{66}}\boldsymbol{\theta}g_2(\mathbf{r},t)+\frac{1}{\rho}\nabla\otimes\nabla\{h_1(\mathbf{r},t)-h_2(\mathbf{r},t)\} \\ &= \lim_{N\to\infty}\sum_{k=1}^{N} w_k\left[\frac{1}{C_{66}}\boldsymbol{\theta}\Phi_2(s_k,\mathbf{r},t)+\frac{1}{\rho}\nabla\otimes\nabla\{\Upsilon_1(s_k,\mathbf{r},t)-\Upsilon_2(s_k,\mathbf{r},t)\}\right] \end{aligned} \tag{97}$$

and

$$\begin{aligned} \boldsymbol{G}_{\mathrm{II}}(\mathbf{r},t) &= \mathbf{e}_3\otimes\mathbf{e}_3\frac{1}{\widehat{C}_{44}}g_3(\mathbf{r},t)+(\mathbf{e}_3\otimes\mathbf{e}_4+\mathbf{e}_4\otimes\mathbf{e}_3)\frac{e_{15}}{\widehat{C}_{44}\eta_{11}}g_3(\mathbf{r},t) \\ &\quad+\mathbf{e}_4\otimes\mathbf{e}_4\left[\frac{e_{15}^2}{\widehat{C}_{44}\eta_{11}^2}g_3(\mathbf{r},t)+\frac{1}{\eta_{11}}g_4(\mathbf{r})\delta(t)\right] \\ &= \lim_{N\to\infty}\sum_{k=1}^{N} w_k\left\{\mathbf{e}_3\otimes\mathbf{e}_3\frac{1}{\widehat{C}_{44}}\Phi_3(s_k,\mathbf{r},t)+(\mathbf{e}_3\otimes\mathbf{e}_4+\mathbf{e}_4\otimes\mathbf{e}_3)\frac{e_{15}}{\widehat{C}_{44}\eta_{11}}\Phi_3(s_k,\mathbf{r},t)\right. \\ &\quad\left.+\mathbf{e}_4\otimes\mathbf{e}_4\left[\frac{e_{15}^2}{\widehat{C}_{44}\eta_{11}^2}\Phi_3(s_k,\mathbf{r},t)+\frac{1}{\eta_{11}}\Psi(s_k,\mathbf{r})\delta(t)\right]\right\} \end{aligned} \tag{98}$$

With (97) and (98) we have determined the *retarded quasi-plane potentials* (15) for a homogeneous spatial density $\rho_s = \Theta_s(\mathbf{r})$ for fiber inclusions with *arbitrary* fiber cross-sections.

6. Dynamic fields of a fiber inclusion with arbitrary cross-section

In the last section we have represented the dynamic electroelastic potentials due to a dynamically transforming inclusion of arbitrary shape with density $\delta(t)\Theta_s(\mathbf{r})$ in series form. In this section we use this result to solve the inclusion problem, i.e. we determine the induced generalized displacement field $\mathscr{U}$ for the quasi-plane transversely isotropic medium. We assume that the inclusion undergoes a uniform eigenstrain $\boldsymbol{\epsilon}^*$ and eigenelectric field $\boldsymbol{E}^*$ of the form (5). The inclusion has the *same* electroelastic moduli $\boldsymbol{C}$, $\boldsymbol{e}$, $\boldsymbol{\eta}$ and mass density ρ as the piezoelectric transversely isotropic matrix material. Taking into account (12) we can write the generalized displacements in the form ($N \to \infty$)

$$\begin{aligned}
u_1 &= \frac{1}{C_{66}} \sum_{m=1}^{N} w_m \left[f_1(\nabla)\Phi_2(s_m,\mathbf{r},t) + \frac{1}{\rho}\left(f_1(\nabla)\frac{\partial^2}{\partial x^2} + f_2(\nabla)\frac{\partial^2}{\partial x \partial y} \right)(\Upsilon_1(s_m,\mathbf{r},t) - \Upsilon_2(s_m,\mathbf{r},t)) \right] \\
u_2 &= \frac{1}{C_{66}} \sum_{m=1}^{N} w_m \left[f_2(\nabla)\Phi_2(s_m,\mathbf{r},t) + \frac{1}{\rho}\left(f_1(\nabla)\frac{\partial^2}{\partial x \partial y} + f_2(\nabla)\frac{\partial^2}{\partial y^2} \right)(\Upsilon_1(s_m,\mathbf{r},t) - \Upsilon_2(s_m,\mathbf{r},t)) \right] \\
u_3 &= \frac{1}{\widehat{C}_{44}} \sum_{m=1}^{N} w_m \left[\left(f_3(\nabla) + \frac{e_{15}}{\eta_{11}} f_4(\nabla) \right) \Phi_3(s_m,\mathbf{r},t) \right] \\
u_4 &= \frac{e_{15}}{\eta_{11}\widehat{C}_{44}} \sum_{m=1}^{N} w_m \left[\left(f_3(\nabla) + \frac{e_{15}}{\eta_{11}} f_4(\nabla) \right) \Phi_3(s_m,\mathbf{r},t) + \delta(t)\frac{f_4(\nabla)}{\eta_{11}} \Psi(s_m,\mathbf{r}) \right]
\end{aligned} \tag{99}$$

where functions Φ_i, Υ_i, Ψ are defined in (91). With (99) we have represented the dynamical generalized displacement fields due to a dynamically transforming fiber inclusion with arbitrary cross-section according to the eigenfields (5) in a form which is useful for numerical evaluation.

7. Numerical examples and visualization

We devote this section to some special cases to confirm the numerical efficiency of the series formulae of (94)–(96).

7.1. Homogeneous fiber inclusions with circular cross-sections

The dynamic potential of a continuous fiber inclusion with circular cross-section (radius a) of unit density $\rho_s(\mathbf{r}) = \Theta(a - r)$ in the space–frequency domain is given by Eqs. (78) and (79) and fulfills

$$(\Delta + \beta^2) g(r,a,\beta) + \Theta(a - r) = 0 \tag{100}$$

For the frequency representation of h defined by (20) we have

$$h(r,a,\beta) = -\frac{1}{c^2\beta^2} g(r,a,\beta) \tag{101}$$

In order to determine the corresponding retarded potentials g, h numerically in the time domain, we use numerical Fourier (Laplace) transformation (Wang, 2001; Wang et al., 2002). To this end we notice that the

frequency domain potentials above are based on the definition of Fourier transform (for example, a function $f(t)$) of

$$\tilde{f}(\omega) = \int_{-\infty}^{\infty} f(t)\mathrm{e}^{\mathrm{i}\omega t}\,\mathrm{d}t$$
$$f(t) = \frac{1}{2\pi}\int_{-\infty}^{\infty} \tilde{f}(\omega)\mathrm{e}^{-\mathrm{i}\omega t}\,\mathrm{d}\omega \tag{102}$$

The potentials g, h in time space domain with infinitesimal damping $\epsilon \to 0+$ become (Wang, 2001; Wang et al., 2002)

$$g(r,a,t) = \lim_{n,M\to\infty} c\frac{\mathrm{e}^{(\epsilon+7\mathrm{i}/2^n)t}}{2^{n+1}\pi}\sum_{k=-M}^{M} g\left(r,a,\mathrm{i}\epsilon+\frac{k-7}{2^n}\right)\mathrm{e}^{-\mathrm{i}tk/2^n}$$
$$h(r,a,t) = \lim_{n,M\to\infty} c\frac{\mathrm{e}^{(\epsilon+7\mathrm{i}/2^n)t}}{2^{n+1}\pi}\sum_{k=-M}^{M} h\left(r,a,\mathrm{i}\epsilon+\frac{k-7}{2^n}\right)\mathrm{e}^{-\mathrm{i}tk/2^n} \tag{103}$$

where M is related to the frequency range of $g(r,a,\beta)$, $h(r,a,\beta)$ and n is related to the time range within which the inverse result has good precision. g_4 defined by (85) is available in closed form (Michelitsch et al., 2002)

$$g_4(r,a) = \frac{1}{4}\Theta(a-r)(2a^2\ln(a) - a^2 + r^2) + \frac{1}{2}\Theta(r-a)a^2\ln(r) \tag{104}$$

Let us now consider the material PZT-5H with the electroelastic moduli

$$\rho = 7500\ \mathrm{kg\,m^{-3}},\quad C_{11}^E = 127\ \mathrm{GPa},\quad C_{44}^E = 23.0\ \mathrm{GPa}$$
$$C_{66}^E = 23.5\ \mathrm{GPa},\quad e_{15} = 17.0\ \mathrm{C\,m^{-2}},\quad \eta_{11} = 1.5\times 10^{-8}\ \mathrm{F\,m^{-1}} \tag{105}$$

Thus, in terms of (21) and (24), we have

$$c_1 \approx 4115\ \mathrm{m\,s^{-1}},\quad c_2 \approx 1770\ \mathrm{m\,s^{-1}},\quad c_3 \approx 2374\ \mathrm{m\,s^{-1}}$$

Fig. 1 shows the propagation of the retarded potential $g_1(r,a,t)$ of a circular source $\delta(t)\Theta(a-r)$. Solid lines represent the numerically generated results of (94) by using (B.4), (B.5) and (B.8) where $a_1 = a_2 = a = 0.1$ m, $N = 100$. The hollow markers represent the results generated by the numerical Fourier transformation (103) by using the exact results for $g_1(r,a,\beta)$ of Eqs. (78) and (79) for a fiber with radius $a = 0.1$ m, $(M = 800, n = 2, \epsilon = 0.002)$. Fig. 1 indicates that the applied numerical method operates with high accuracy. In the internal space $g_1(r,a,t)$ shows linear behavior of $g_1(r,a,t) = c_1^2 t$ for $t < t_0 = (a-r)/c$ which is in accordance with the exact result (below Eq. (106)). [14] Moreover, it can be seen in Fig. 1 that g_1 is in the outside space $r > a$ a circular (cylindrical) wave package propagating with wave speed c_1, arriving at a circle r in the external space when $t = (r-a)/c$ is equal the runtime from the circle r to the closest source point being located on the boundary of the fiber. A speciality of the 2D medium is that once the wave package has reached a certain circle r, the amplitude will remain non-zero $\forall t > (r-a)/c_1$. This non-zero tail of a wave package uniformly emitted due to a density $\Theta(a-r)\delta(t)$ is a consequence of the retarded 2D Green's function $\hat{g} = 1/\Theta(t-R/c)/(2\pi\sqrt{t^2-(R/c)^2})$ non-vanishing $\forall t > R/c$. This is in contrast to the 3D case where the amplitude is vanishing for times greater than the runtime from the spacepoint to the furthermost source point. [15]

[14] This remarkable property also occurs in the 3D case.

[15] This is a consequence of the 3D retarded Green's function $\hat{g}_3(R,t) = \delta(t-R/c)/(4\pi R)$ which contributes only for $R = ct$. For an extensive discussion of these runtime effects and a comparison of the 2D and 3D case we refer to our recent paper Wang et al. (2003).

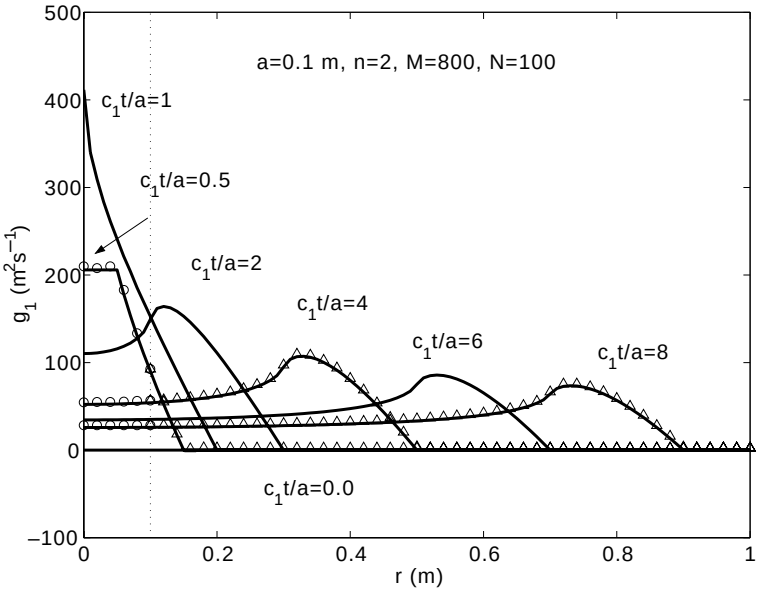

Fig. 1. Time evolution of the retarded potential $g_1(r,a,t)$ of a solid circular source. Solid lines represent the results of (94), by using (B.4) and (B.5) with $a_1 = a_2 = a = 0.1$ m, $N = 100$. Hollow markers represent the result generated by using the closed-form results of (78) and (79) in (103) ($a = 0.1$ m, $M = 800$, $n = 2$, $\epsilon = 0.002$).

Fig. 2 represents the 3D plot of the propagation of the same retarded potential $g_1(r,a,t)$ as in Fig. 1. The plot shows the linear behavior in the internal space as well as the propagation of the wave front. The non-zero tail for increasing time t is also indicated.

Fig. 3 shows the propagation of the potential $h_2(r,a,t)$ of the same circular inclusion as in Figs. 1 and 2. Solid lines represent the results of (95) using (B.4), (B.5) and (B.8) with $a_1 = a_2 = a = 0.1$ m, $N = 100$. Hollow markers represent the same potential generated by (103) with $(M = 800, n = 2, \epsilon = 1)$ by integrating the exact dynamic potential (Eqs. (78) and (79)).

Fig. 4 shows the Newtonian potential $g_4(r,a)$ of the circular inclusion of Fig. 3 ($a = 0.1$ m). Solid lines represent the results generated by (96) using (B.4) and (B.5) with $N = 100$. Hollow markers represent the same potential generated by the exact formula (104).

These examples show high accuracy agreement between the numerical time domain Fourier integrals of the close form solutions (78) and (79) and the numerically generated results based on formulae (94) and (95). Furthermore, the numerical evaluation of (96) approximates the exact Newtonian potential (104) with high accuracy.

7.2. Homogeneous elliptical fiber inclusion

Consider the maximum value of potential g_i. It is reasonable that the maximum should appear when the spacepoint is located inside the source region with $\alpha = 0$, $\beta = 2\pi$ and $P_l(\theta,\mathbf{r}) = 0$, i.e., $H_{il} = 0$. Now, let us consider the function Φ_i of (91). Thus, we have $\max(\Phi_i) = \frac{c_i^2 t}{2\pi}$ as function of t when $H_{iu} = c_i t$, i.e., the circle $r_s = c_i t$ is still inside the source region or $c_i t \leqslant P_u$. Thus we find the remarkable properties

$$g_i(\mathbf{r},t) = \Theta(t_0(\mathbf{r}) - t)\int_\alpha^\beta \mathrm{d}\theta \Phi_i(\theta,\mathbf{r},t) = \int_0^{2\pi} \mathrm{d}\theta \frac{c_i^2 t}{2\pi} = c_i^2 t, \quad t \in [0, t_0(\mathbf{r})] \tag{106}$$

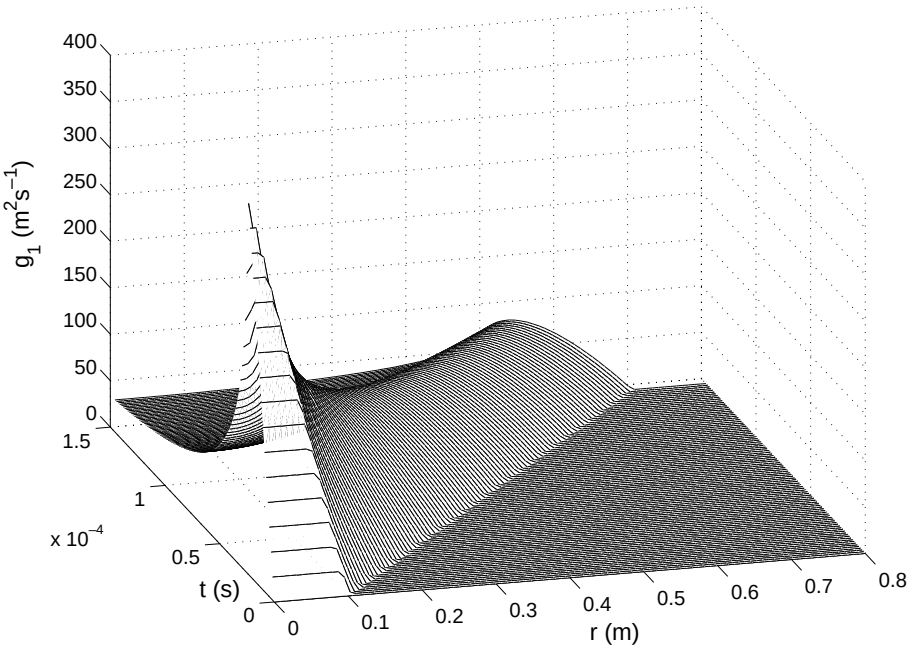

Fig. 2. 3D plot of the propagation of the retarded potential $g_1(r,a,t)$ of Fig. 1 generated by Eqs. (94) with $a = a_1 = a_2 = 0.1$ m, $N = 100$.

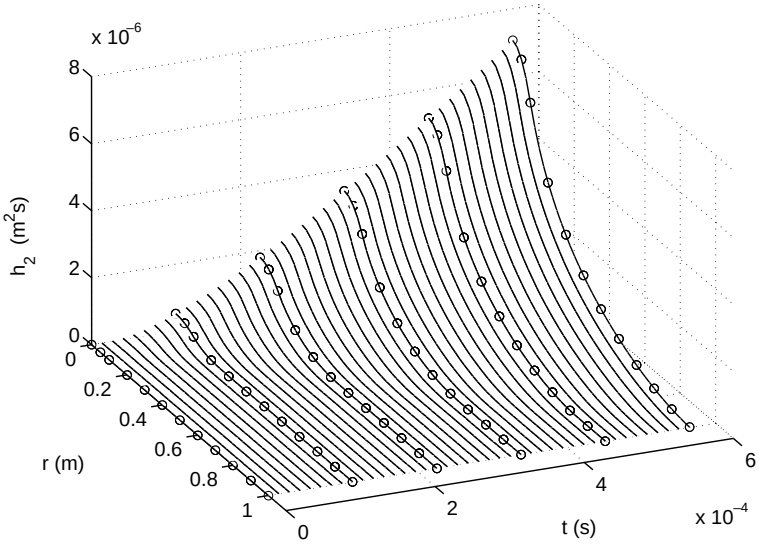

Fig. 3. Propagation of the potential $h_2(r,a,t)$ of the same inclusion as in Figs. 1 and 2. Solid lines represent the results of (95) with $a_1 = a_2 = a = 0.1$ m, $N = 100$. Hollow markers represent the results generated by (103) $(M = 800, n = 2, \epsilon = 1)$ together with (101) by using the exact solutions for $g(r,a,\beta)$ of Eqs. (78) and (79).

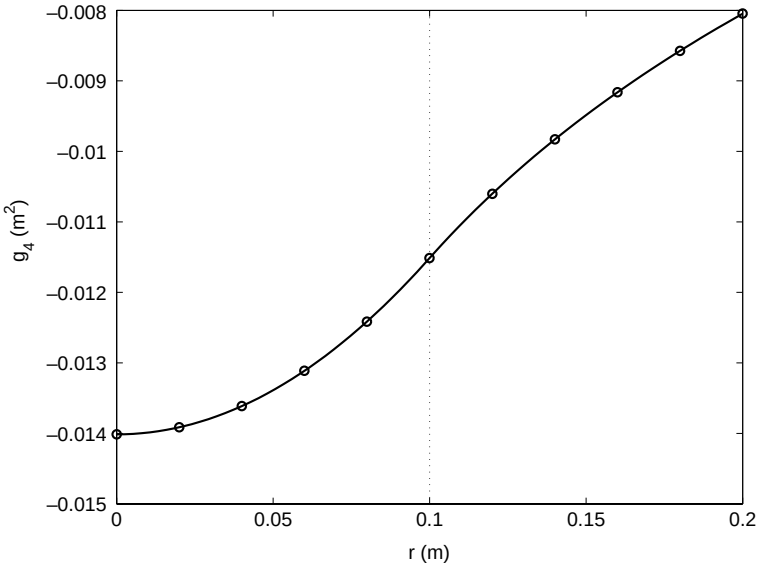

Fig. 4. Newtonian potential $g_4(r,a)$ of a homogeneous circular source $\Theta(a-r)$. Solid lines represent the numerical result of (96) (by using (B.4), (B.5) and (B.8)) with $a_1 = a_2 = a = 0.1$ m, $N = 100$. Hollow markers represent the exact results given by (104) with $a = 0.1$ m.

$$h_i(\mathbf{r},t) = \Theta(t_0(\mathbf{r}) - t)\int_\alpha^\beta \mathrm{d}\theta \Upsilon_i(\theta,\mathbf{r},t) = \int_0^{2\pi} \mathrm{d}\theta \frac{c_i^2 t^3}{12\pi} = \frac{1}{6}c_i^2 t^3, \quad t \in [0, t_0(\mathbf{r})] \tag{107}$$

where $t_0(\mathbf{r}) = \frac{\min_\theta[P_u(\mathbf{r},\theta)]}{c_i}$. Eqs. (106) and (107) remain also true for fiber inclusions with arbitrary cross-sections and in the 3D case of an inclusion of arbitrary shape. In the time range $0 < t < t_0(\mathbf{r})$ waves arrive at $\mathbf{r}$ emitted from circles with radii $c_i t$ around $\mathbf{r}$ being completely inside the inclusion. Since in this time range no waves arrive at $\mathbf{r}$ which are emitted from boundary points, g_i, h_i are *independent* on a_i. This effect takes place *uniformly* for all $\mathbf{r}$ inside the inclusion, thus also the $\mathbf{r}$-dependence is absent for $0 < t < t_0(\mathbf{r})$. The analogue observation is also true for 2D homogeneous inclusions with arbitrary boundaries.

In a sense this dynamical effect which also holds in the 3D case, can be regarded as the dynamical counterpart to the static Eshelby theorem (according to which the strains inside an elliptical inclusion are of the same polynomial order than the eigenstrains). [16] Moreover, for any internal spacepoint the maximum value of g_i is taken when $t = t_0(\mathbf{r})$ and therefore the absolute maximum value of g_i is taken at the *furthermost internal spacepoint* from the boundary of the inclusion. This is true for 2D inclusions with arbitrary boundaries. Since $\max_r(t_0(\mathbf{r})) = \max_r[\frac{\min_\theta[P_u(\mathbf{r},\theta)]}{c_i}]$, we get

$$\max_{rt}[g_i(\mathbf{r},t)] = c_i \max_r[\min_\theta(P_u(\mathbf{r},\theta))]$$

For the elliptical inclusion, we get

$$\max_{rt}[g_i(\mathbf{r},t)] = c_i \min(a_1,a_2)$$

where a_1, a_2 are semi-axes of the ellipse.

[16] The 2D and 3D cases are discussed in our recent paper, Wang et al. (2003).

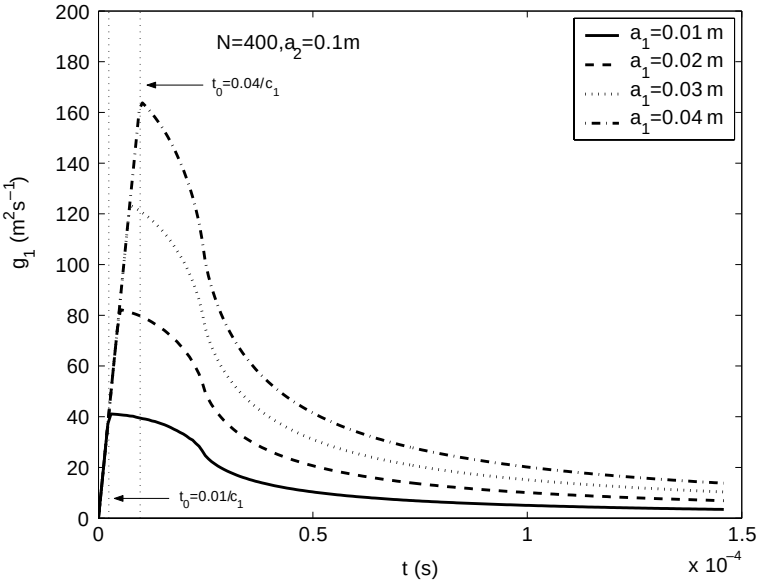

Fig. 5. Time evolution of $g_1(\mathbf{r},t)$ at the origin $\mathbf{r}=(0,0)$ of an ellipsoidal source region (density $\delta(t)\Theta(1-p)$) with semi-axis $a_2=0.1$ m generated by (94) for varying axis $a_1=0.01$, 0.02, 0.03, 0.04 m, $N=400$.

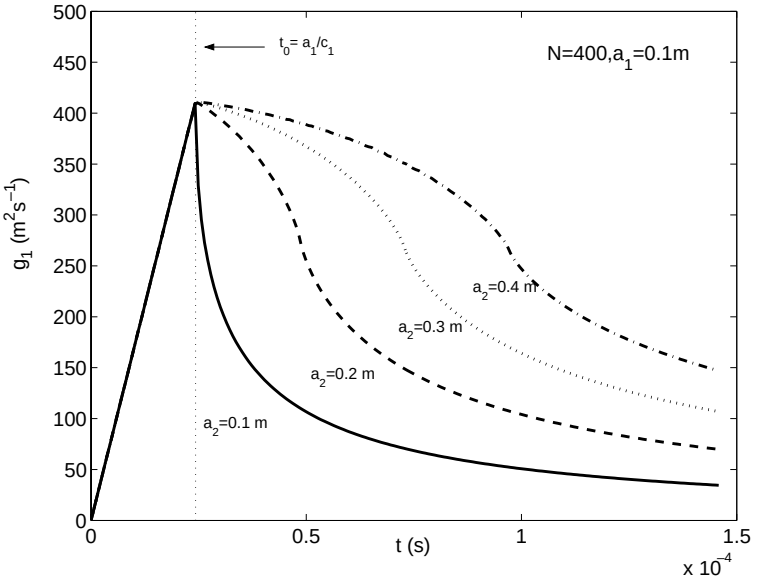

Fig. 6. Time evolution of potential $g_1(\mathbf{r},t)$ in the origin $\mathbf{r}=(0,0)$ of an ellipsoidal source (density $\delta(t)\Theta(1-p)$) with $a_1=0.1$ m ((94) with (B.4) and (B.5)) and varying $a_2=0.1$, 0.2, 0.3, 0.4 m, and $N=400$.

Figs. 5 and 6 show the time evolution of potential $g_1(\mathbf{r},t)$ in the origin $\mathbf{r}=0$ of a fiber inclusion for elliptical cross-section generated by ((94) together with (B.4), (B.5) and (B.8)) (density $\delta(t)\Theta(1-p)p^2=\frac{x^2}{a_1^2}+\frac{y^2}{a_2^2}$, respectively). In Fig. 5 the semi-axis $a_2=0.1$ m is fixed and semi-axis $a_1=0.01$,

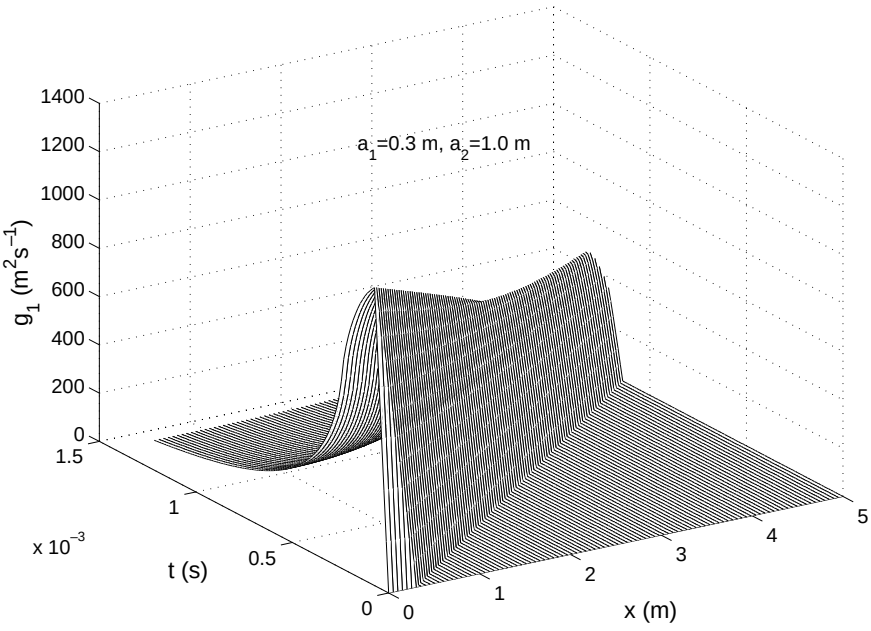

Fig. 7. 3D plot of the propagation of the potential $g_1(\mathbf{r}, t)$ (Eqs. (94) with (B.4), (B.5) and (B.8) with $a_1 = 0.3$ m, $a_2 = 1.0$ m, $N = 400$) of an ellipsoidal source region (density $\delta(t)\Theta(1-p)$).

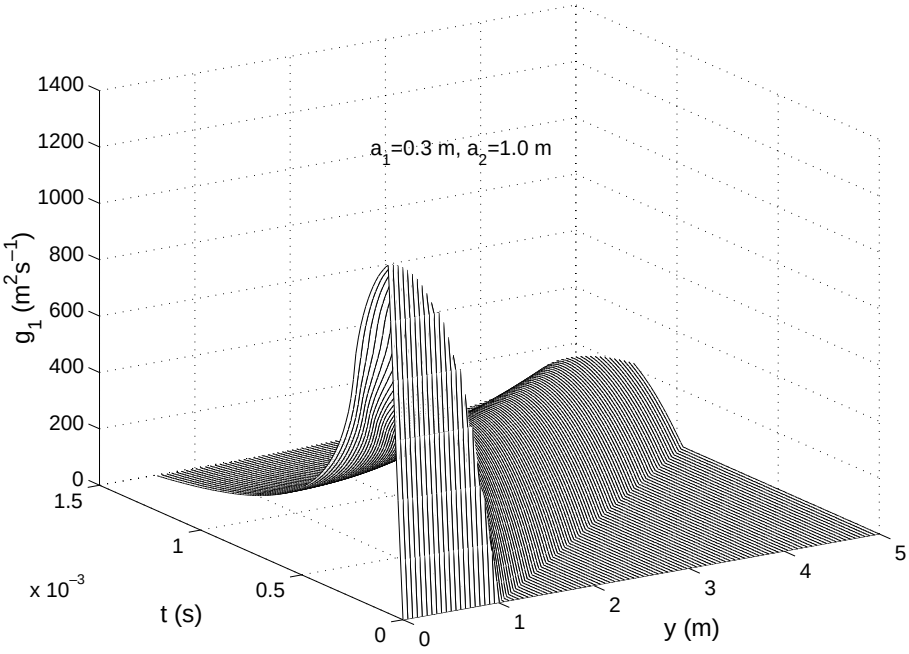

Fig. 8. 3D plot of the propagation of the same potential as in Fig. 7 along the $\mathbf{r} = (0, y)$-direction.

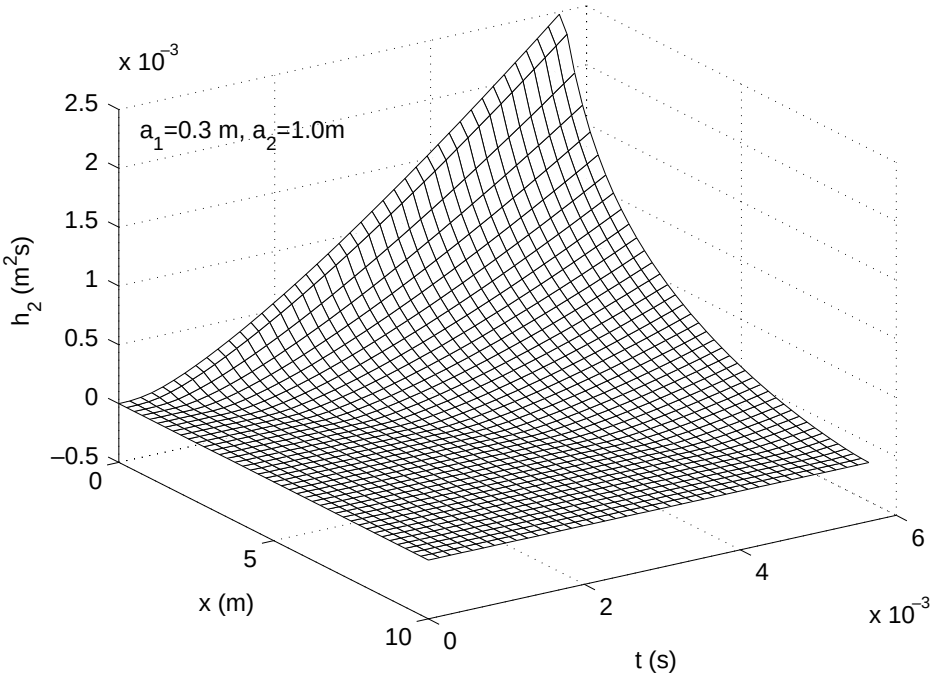

Fig. 9. 3D plot of the propagation of potential $h_2(\mathbf{r}, t)$ (Eqs. (95) with (B.4), (B.5) and (B.8)) of the same source density as in Figs. 7 and 8.

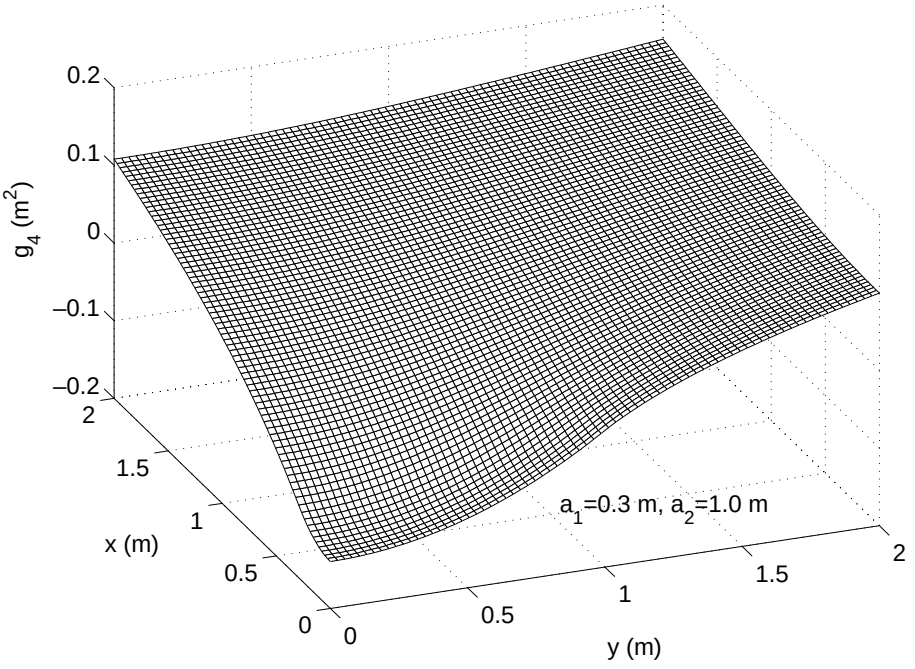

Fig. 10. 3D plot of the Newtonian potential $g_4(\mathbf{r})$ (Eqs. (96), with (B.4), (B.5) and (B.8)) with $a_1 = 0.3$ m, $a_2 = 1.0$ m of the same ellipsoidal inclusion as Figs. 8 and 9 with density $\Theta(1-p)$ in which $N = 400$.

0.02, 0.03, 0.04 m is varied. In Fig. 6 $a_1 = 0.1$ m is fixed and $a_2 = 0.1$, 0.2, 0.3, 0.4 m is variable. These Figs. indicate that for $t < t_0 = \min(a_1, a_2)/c$ the retarded potential shows linear behavior independent on the semi-axes a_i as indicated by the exact Eq. (106). For both cases in the linear range, the slope is equal to c_1^2. Moreover, g_1 takes its maximum value $g_1(0, t_0) = c_1 \min(a_1, a_2)$ in the center of the ellipse ($r = 0$).

Figs. 7 and 8 show 3D plots of the propagation of the retarded potential $g_1(\mathbf{r}, t)$ for an elliptical inclusion (source density $\delta(t)\Theta(1-p)$, $a_1 = 0.3$ m, $a_2 = 1.0$ m) in x- and y-directions, respectively. The plots are generated by employing Eqs. (94) together with (B.4), (B.5) and (B.8).

Fig. 9 shows the 3D plot of the propagation in $(x, 0)$-direction of the potential $h_2(\mathbf{r}, t)$ for the same elliptical inclusion as in Figs. 7 and 8 where Eqs. (95) with (B.4), (B.5) and (B.8) have been used.

Fig. 10 shows the 3D plot of a Newtonian potential $g_4(\mathbf{r})$ generated by Eq. (96) using (B.4), (B.5) and (B.8) of the same elliptical inclusion as in Figs. 7–9.

The above examples demonstrate the interplay of runtime and superposition effects. Moreover, all of these examples show high precision agreement of the purely numerically generated results and the results where closed-form solutions are involved.

8. Conclusions

In the present paper the dynamic electroelastic fields (displacements and electric potential) in a transversely isotropic medium with dynamically transforming continuous fiber inclusion are studied. The dynamic fields are expressed in terms of three types of scalar functions, namely the retarded potential g defined by (19), the related potential h of (20) and the Newtonian potential g_4 defined by (25). The latter does not affect the wave propagation.

By means of Fourier transformation compact integral formulae are derived for the dynamic and retarded potentials of continuous fiber inclusions with elliptical cross-sections and continuous fiber tubes (Eqs. (47)ff.). For special cases (circular fiber inclusions and fiber tubes) known closed-form expressions (Michelitsch et al., 2002, 2003a) are reproduced.

For fiber inclusions with arbitrary cross-sections a numerical procedure is applied based on Gauss quadrature technique. The numerically evaluated dynamic and retarded potentials determine completely the generalized displacements (displacements and electric potential). The numerical solution is obtained in terms of simple scalar functions (expressions (91), (94)–(96), respectively). The efficiency and high accuracy of the numerical procedure is confirmed in Section 7 by means of a circular inclusion. Characteristic propagation and runtime effects are found analytically and numerically. For the retarded potential g of a homogeneous density $\delta(t)\Theta_s(\mathbf{r})$ they can be summarized as follows: (i) For times being smaller than the runtime from the spacepoint $\mathbf{r}$ to the closest boundary point the behavior in the internal space is governed by a *uniform* linear increase with time being independent on $\mathbf{r}$ and the geometric characteristics (shape) of the source region. (ii) g takes its maximum value in the furthermost internal spacepoint from the boundary. The maximum occurs at the time being the runtime from this spacepoint to the closest boundary point (e.g. for a circular inclusion in its center). (iii) For an external spacepoint g is non-vanishing only for times greater than the runtime to the closest boundary point. (i)–(iii) are also true in the corresponding 3D case as recently found by Wang et al. (2003). (iv) Unlike in the 3D case, in the 2D case once the wave has arrived, $g > 0$ remains non-vanishing for all times greater than this runtime. (i)–(iv) are true for continuous fiber inclusions of *arbitrary cross-sections* with source density $\delta(t)\Theta_s(\mathbf{r})$. (iii) and (iv) remain true even for inhomogeneous densities $\delta(t)\Theta_s(\mathbf{r})\rho_s(\mathbf{r})$ whereas (i) and (ii) have to be modified. [17]

[17] A discussion of inhomogeneous densities of the 3D case can be found in our recent paper, Wang et al. (2003).

The present results and approaches are useful for the solution of a wide range of dynamical engineering problems in the 2D piezoelectric space (corresponding to a 3D transversely isotropic medium with fiber inclusions). They can be applied in self consistent models to determine the effective dynamic material properties and are useful for the description of wave propagation phenomena in piezoelectric fiber composites.

Acknowledgement

Financial support by the Deutsche Forschungsgemeinschaft (DFG), project no. GA732/1-1 is gratefully acknowledged.

Appendix A

In this appendix we give a proof for Eq. (45). To that end we consider ($\mathbf{k} = k\hat{\mathbf{k}}$)

$$I = \int_{|\hat{\mathbf{k}}|=1} f(\hat{k}_i)\,\mathrm{d}\Omega(\hat{\mathbf{k}}) = \int_{|\hat{\mathbf{k}}|=1} f(\hat{k}_i)\hat{\mathbf{k}}\cdot\hat{\mathbf{k}}\,\mathrm{d}\Omega(\hat{\mathbf{k}}) \tag{A.1}$$

by using Gauss' theorem this integral can be rewritten as

$$I = \int_{k^2<1} f(\hat{k}_i)\,\mathrm{d}\Omega(\hat{\mathbf{k}}) = \int_{|\hat{\mathbf{k}}|=1} \nabla_{\mathbf{k}}(\mathbf{k} f(\hat{k}_i))\,\mathrm{d}^2\mathbf{k} \tag{A.2}$$

Now we put $k_i = \frac{K_i}{a_i} = K\frac{\widehat{K}_i}{a_i}$ ($\sum_i \widehat{K}_i^2 = 1$). The region $k^2 = K^2\sum_i \frac{\widehat{K}_i^2}{a_i^2} < 1$ is characterized by $K(\widehat{\mathbf{K}}) \leqslant s(\widehat{\mathbf{K}}) = 1\Big/\sqrt{\sum_i \frac{\widehat{K}_i^2}{a_i^2}}$. Thus I becomes

$$I = \frac{1}{a_1 a_2}\int_{|\widehat{\mathbf{K}}|=1} \mathrm{d}\Omega(\widehat{\mathbf{K}}) \int_0^{s(\widehat{\mathbf{K}})} \frac{\mathrm{d}}{\mathrm{d}K}\left(K^2 f\left(K\frac{\widehat{K}_i}{a_i}\right)\right)\mathrm{d}K \tag{A.3}$$

which yields after the K-integration (45)

$$I = \frac{1}{a_1 a_2}\int_{|\widehat{\mathbf{K}}|=1} f\left(\frac{\widehat{K}_i}{a_i}s(\widehat{\mathbf{K}})\right)s^2(\widehat{\mathbf{K}})\,\mathrm{d}\Omega(\widehat{\mathbf{K}}) \tag{A.4}$$

Appendix B

We consider an elliptical fiber inclusion with boundary shape characterized by

$$F(\mathbf{r}') = \frac{x'^2}{a_1^2} + \frac{y'^2}{a_2^2} - 1 = 0 \tag{B.1}$$

With spacepoint $\mathbf{r} = (x, y)$ and $\mathbf{s} = (x_s, y_s) = \mathbf{r}' - \mathbf{r}$, we have $\mathbf{r}' = \mathbf{s} + \mathbf{r}$ thus (B.1) becomes

$$F(\mathbf{s}+\mathbf{r}) = \frac{(x_s + x)^2}{a_1^2} + \frac{(y_s + y)^2}{a_2^2} - 1 = 0 \tag{B.2}$$

By putting $x_s = r_s\cos(\theta)$, $y_s = r_s\sin(\theta)$, we can express the boundary of the region $F(\mathbf{s}+\mathbf{r})$ in polar coordinates as

$$r_s = \frac{-a_1^2 y \sin(\theta) - a_2^2 x \cos(\theta) \pm \sqrt{Q}}{a_1^2 \sin^2(\theta) + a_2^2 \cos^2(\theta)} \tag{B.3}$$

where $Q = a_1^2 a_2^2 [-(y\cos(\theta) - x\sin(\theta))^2 + a_1^2 \sin^2(\theta) + a_2^2 \cos^2(\theta)]$. Notice that $\frac{\sqrt{Q}}{a_1^2 \sin^2(\theta) + a_2^2 \cos^2(\theta)} \geqslant 0$, therefore

$$P_u = \frac{-a_1^2 y \sin(\theta) - a_2^2 x \cos(\theta) + \sqrt{Q}}{a_1^2 \sin^2(\theta) + a_2^2 \cos^2(\theta)} \tag{B.4}$$

For the internal space we have $\alpha = 0$, $\beta = 2\pi$ for the lower and upper limits of the angle and $P_l = 0$ for the lower limit of the radius r_s. On the other hand, if the spacepoint is located outside the source region, the lower limit of radius coordinate is

$$P_l = \frac{-a_1^2 y \sin(\theta) - a_2^2 x \cos(\theta) - \sqrt{Q}}{a_1^2 \sin^2(\theta) + a_2^2 \cos^2(\theta)} \tag{B.5}$$

To obtain the lower and upper angle limits α, β, we put $Q = 0$ which leads to

$$\tan(\theta) = \left(\frac{-xy \pm \sqrt{-a_1^2 a_2^2 + a_2^2 x^2 + a_1^2 y^2}}{a_1^2 - x^2} \right) \tag{B.6}$$

thus

$$\begin{aligned} \gamma_1 &= \arctan\left(\frac{-xy + \sqrt{-a_1^2 a_2^2 + a_2^2 x^2 + a_1^2 y^2}}{a_1^2 - x^2} \right) \\ \gamma_2 &= \arctan\left(\frac{-xy - \sqrt{-a_1^2 a_2^2 + a_2^2 x^2 + a_1^2 y^2}}{a_1^2 - x^2} \right) \end{aligned} \tag{B.7}$$

where $-\pi/2 \leqslant \gamma_1, \gamma_2 \leqslant \pi/2$. In view of the symmetry of the inclusion we have to consider only spacepoints which satisfy $x > 0$, $y > 0$ being located outside the inclusion. For this case the lower and upper limits of angle coordinate satisfy $\pi/2 < \alpha < 3\pi/2$, $\pi < \beta < 2\pi$, which together with (B.7) leads to

$$\begin{aligned} \alpha &= \pi + \gamma_1 \\ \beta &= \pi - \frac{1}{2}\pi \mathrm{sign}(\gamma_2)[1 - \mathrm{sign}(\gamma_2)] + \gamma_2 \end{aligned} \tag{B.8}$$

References

Cheng, Z.Q., Batra, R.C., 1999. Exact Eshelby tensor for a dynamic circular cylindrical inclusion. J. Appl. Mech. 66, 563–565.

Courant, R., Hilbert, D., 1989. In: Methods of Mathematical Physics, vol. I. Wiley.

Davis, P.J., Rabinowitz, P., 1984. Methods of Numerical Integration. Academic Press, New York.

Dyson, F.D., 1891. The potentials of ellipsoids of variable densities. Q. J. Pure Appl. Math. XXV, 259–288.

Eshelby, J.D., 1957. The determination of the elastic field of an ellipsoidal inclusion, and related problems. Proc. R. Soc. Lond. A 241, 376–396.

Ferrers, N.M., 1877. On the potentials of ellipsoids, ellipsoidal shells, elliptic laminae and elliptic rings of variable densities. Q. J. Pure Appl. Math. 14, 1–22.

Jackson, J.D., 1999. Classical Electrodynamics, third ed. Wiley, New York, p. 1999.

Levin, V.M., Michelitsch, T.M., Gao, H., 2002. Propagation of electroacoustic waves in the transversely isotropic piezoelectric medium reinforced by randomly distributed cylindrical inhomogeneities. Int. J. Solids Struct. 39, 5013–5051.

Michelitsch, T.M., Levin, V.M., Gao, H., 2002. Dynamic potentials and Green's functions of a quasi-plane piezoelectric medium with inclusion. Proc. R. Soc. Lond. A 458, 2393–2415.

Michelitsch, T.M., Gao, H., Levin, V.M., 2003a. Dynamic Eshelby tensor and potentials for ellipsoidal inclusions. Proc. R. Soc. Lond. A 459, 863–890.

Michelitsch, T.M., Gao, H., Levin, V.M., 2003b. On the dynamic potentials of ellipsoidal shells. Q. J. Mech. Appl. Math. 57 (1), 1–20.

Mikata, Y., Nemat-Nasser, S., 1990. Elastic field due to a dynamically transforming spherical inclusion. J. Appl. Mech. ASME 57, 845–849.

Pao, Y.H., 1978. In: Elastic Waves and Non-Destructive Testing of Material. Applied Mechanics Division, vol. 29. American Society of Engineers, New York.

Press, W.H., Teukolski, S.A., Vetterling, W.T., Flannery, B.P., 1992. Numerical Recipes in Fortran 77: the art of Scientific Computing, second ed. Cambridge University Press.

Rahman, M., 2002. The isotropic ellipsoidal inclusion with a polynomial distribution of eigenstrain. J. Appl. Mech.—Trans. ASME 69 (5), 593–601.

Routh, E.J., 1982. A Treatise On Analytic Statics, Vol. 2 (Cambridge University Press).

Talbot, D.R.S., Willis, J.R., 1983. Variational estimates for dispersion and attenuation of waves in random composites—III. Int. J. Solids Struct. 19 (9), 793–811.

Wang, J., 2001. Generalized Theory and Arithmetic of Orthogonal Wavelets and Applications to Researches of Mechanics Including Piezoelectric Smart Structures. Ph.D. Thesis, Lanzhou University (in Chinese).

Wang, J., Zhou, Y.H., Gao, H., 2002. Computation of the Laplace inverse transform by wavelet theory. Commun. Numer. Meth. Engng., in press.

Wang, J., Michelitsch, T.M., Gao, H., 2003. On the retarded potentials and related solutions of the inhomogeneous wave- and Helmholtz equation of ellipsoids, shells and sources of arbitrary shapes, to be published.